Title

The transformation of U(VI) and V(V) in carnotite group minerals during dissimilatory respiration by a metal reducing bacterium

Authors

Glasauer, Susan

Fakra, Sirine C

Schooling, Sarah

et al.

Publication Date

2022-03-01

DOI

10.1016/j.chemgeo.2022.120726

The transformation of U(VI) and V(V) in carnotite group minerals during dissimilatory respiration by a metal reducing bacterium

Authors: Susan Glasauer[1*], Sirine C. Fakra[2], Sarah Schooling[1], Peter Weidler[3], Tolek Tyliszczak[4], David K. Shuh[4]

1. School of Environmental Sciences, University of Guelph, Guelph, ON N1G 2W1, Canada

2. Advanced Light Source, Lawrence Berkeley National Laboratory, Berkeley, CA 94720, USA.

3. Institute of Functional Interfaces, Karlsruhe Institute of Technology, Karlsruhe, Germany

4. Chemical Sciences Division, Lawrence Berkeley National Laboratory, Berkeley, CA 94720, USA.

*corresponding author: glasauer@uoguelph.ca

KEYWORDS: metal reduction, *Shewanella*, carnotite, uranium, vanadium, Scanning Transmission X-ray Microscopy.

For Chemical Geology

ABSTRACT

Recent results from laboratory and field studies support that dissimilatory metal reducing (DMR) bacteria influence the fate and transport of uranium in anaerobic subsurface environments. To date, most research efforts have focused on the reduction of soluble U(VI) by DMR bacteria to form insoluble uraninite (UO_2). Subsurface environments harbor, however, large reservoirs of U(VI) in solid or mineral form. Uranium that is structure-bound in minerals is expected to be more refractory to microbial reduction than soluble U, based on analogy with Fe respiration. The reducibility of U(VI) could impact the fate of U(IV) by controlling mineral precipitation reactions, which has implications for the long-term immobilization of U in subsurface environments. We studied anoxic cultures of *Shewanella putrefaciens* CN32 incubated with natural carnotite-group minerals by X-ray diffraction, electron microscopy, scanning transmission X-ray microscopy (STXM). Near-edge X-ray absorption fine structure (NEXAFS) spectroscopy measurements at U-$N_{4,5}$, V-$L_{2,3}$, and O-K edges on cultures incubated up to 10 months show that V(V) was reduced to V(IV), whereas U was not reduced. In contrast, V(V) and U(VI) in solution were both completely reduced to lower oxidation states by CN32, as precipitates within the exopolymer surrounding the bacteria. Assays for the toxicity of U and V to CN32 showed that biofilm formation was stimulated at 0.001 M U(VI), and growth was inhibited at concentrations of U(VI) greater than 0.001 M. Vanadium did not inhibit growth or stimulate biofilm formation at any concentration tested. Investigations of the bacteria-mineral and bacteria-metal interface at the nanometer and molecular scales provide new insights into the co-respiration of V and U that help explain their biogeochemical cycling and have implications for subsurface bioremediation of these elements.

1.0 INTRODUCTION

The most important ore minerals of the Colorado Plateau uranium deposits belong to the uranyl vanadate group, also known as carnotite group minerals (CGM). These include carnotite [$K_2(UO_2)_2(V_2O_8)(H_2O)_3$] and tyuyamunite [$Ca(UO_2)_2(V_2O_8)(H_2O)_8$], which consist of uranyl divanadite $(V_2O_8)^{6-}$ layer complexes that are analogous to layer silicates and contain cations in the interlayer positions (Evans and White, 1987). The ability of uranyl vanadate minerals to accommodate different interlayer cations explains the wide range of possible compositions (Evans and Garrels, 1958; Evans and White, 1987; Finch and Murakami, 1999). The Colorado Plateau ores were processed for radium, vanadium and uranium since the late 19th century (Thews and Heinle, 1923; Weeks, 1961), leaving legacies of tailings. Although they are considered insoluble under the slightly alkaline, oxidizing conditions that dominate Colorado Plateau surface environments today (Evans and Garrels, 1958; Langmuir, 1978), extraction activity has resulted in areas of elevated concentrations in Utah and Colorado as well as in other locations where U was processed.

The reduction of soluble U(VI) by some bacteria is well documented (e.g., Lovely et al., 1991; Haas and DiChristina, 2002; Lloyd et al., 2002; Lloyd and Renshaw, 2005; reviewed in Kolhe et al., 2018). Bioremediation strategies that center on manipulating the activities of dissimilatory metal reducing (DMR) bacteria have been explored for the removal of U(VI) from groundwater, perhaps most notably at Rifle, CO (e.g., Xu et al., 2017; Bargar et al., 2013; Williams et al. 2011; Zhuang et al., 2012; Li 2010; Vrionis et al., 2005; Ortiz Bernad et al., 2004b; Anderson et al., 2003). Subsurface bioremediation strategies are based on the reduction of U(VI) species to relatively insoluble hydroxylated uranate complexes (Langmuir, 1978; Bargar et al., 2013; Stylo et al., 2013). In contrast to studies with soluble U(VI), the ability of DMR bacteria to reduce U(VI) that is present in natural minerals has received less attention. This is a

71 striking gap in the understanding of how bacteria may transform U, given that solid mineral
72 phases are the largest reservoirs of metals in weathering environments, as well as the ultimate
73 sinks. Several synthetic U(VI) mineral analogs have been shown to be reducible by dissimilatory
74 bacteria, including: metaschoepite [$UO_3 \cdot 2H_2O$] (Fredrickson et al., 2000), uramphite
75 [$(NH_4)(UO_2)(PO_4) \cdot H_2O$] (Khijniak et al., 2005), synthetic U(VI) borate and boronate crystals
76 (Yang et al., 2014), and natural boltwoodite [$HK(UO_2)(SiO_4) \cdot H_2O$ (Liu et al, 2006; Liu et al.,
77 2009). In one study, the U(VI) contained in meta-autunite ($Ca[(UO_2)(PO_4)](H_2O)_6$) could not be
78 reduced by DMR bacteria (Smeaton et al., 2008). The U(VI) minerals in these studies are,
79 however, much less widespread than for CGM, which are associated with roll front deposits in
80 the Colorado Plateau and in Australia (reviewed in Cumberland, 2016).
81 The V(V) contained in CGM is another possible electron acceptor. Given its favorable
82 solution and redox chemistry (Wehrli and Stumm, 1989; Huang et al., 2016), vanadium should
83 compete effectively with U(VI) for electrons produced during respiration by DMR bacteria. The
84 aqueous chemistry of vanadium is complex due to multiple oxidation states and strong tendencies
85 to hydrolyze and polymerize (Macara, 1980; Rehder, 2008). Vanadate ions ($H_2VO_4^-$ and HVO_4^-)
86 are relatively stable under oxidizing conditions, exhibiting chemical behavior similar to
87 phosphate. Vanadyl (VO^{2+}) species are found in reducing environments and are typically more
88 insoluble than vanadate ions (Eckstrom et al., 1983; Premovic et al., 1986). Trivalent V occurs in
89 complexes of low solubility under strongly reducing, i.e., sulfidic, conditions (Wehrli and
90 Stumm, 1989). Several bacterial species have been shown to reduce soluble V(V) to V(IV),
91 including *Shewanella oneidensis* and *Geobacter metallireducens* (Lyalikova and Yurkova, 1992;
92 Carpentier et al., 2003, 2005; Ortiz-Bernad et al., 2004a), as well as a native microbial
93 community (Hao et al., 2018). There is just one report of reduction to V(III) (Li et al., 2007). To

94 the best of our knowledge, the bacterial reduction of solid or mineral-bound V has not been
95 investigated.
96 Bacteria introduce complexity to geochemical reactions by their ability to establish micro
97 and nanoscale chemical gradients (Hunter and Beveridge, 2005). To investigate the bioreactivity
98 of mineral U and V, we incubated anoxic cultures of *Shewanella putrefaciens* CN32 with natural
99 CGM contained in U ore associated with sandstone and examined the products using nanoscale
100 synchrotron-based X-ray spectromicroscopy techniques. *S. putrefaciens* CN32 is known to
101 reduce U as well as Fe and other transition metals (reviewed in DiChristina et al., 2005). Because
102 CN32 was originally isolated from Colorado Plateau deposits, it is a relevant model organism for
103 investigating biological contributions to the terrestrial cycling of metals in this environment.
104 Our investigations were centered on testing: 1) whether the presence of V(V), an alternate
105 electron acceptor, will inhibit the reduction of U(VI) by DMR bacteria; 2) whether the chemical
106 phase of U and V, i.e., solid vs. soluble, will affect bacterial dissimilatory reduction and
107 associated mineral products, and 3) bacterial growth responses to U and V. To characterize the
108 samples, we used soft X-ray scanning transmission X-ray microscopy (STXM), electron
109 microscopy, X-ray diffraction and wet chemical techniques. Elemental mapping (C, K, Ca, O,
110 Mn, Fe, V, U and Ba) and NEXAFS spectroscopy at U 4f, V 2p and O1s edges were performed
111 using STXM on minerals and bacteria samples over the 10-month incubation period, in both dry
112 and hydrated sample conditions. The combination of bulk analyses with spectromicroscopic
113 techniques at the nanoscale allowed us to capture the small-scale heterogeneity induced by active
114 bacteria as well as the relative magnitude of the observed changes in mineralogy.
115
116 **2.0 MATERIALS AND METHODS**
117 **2.1 Materials**

118 Material from a stockpile of unprocessed uranium ore was obtained from southeastern
119 Utah, where it is associated with roll front and tabular deposits of the Colorado Plateau (Weeks,
120 1961; Finch and Murakami, 1999). The uranium minerals occur as coatings on consolidated
121 sandstone that is porous and friable, which we identified using XRD. The metal concentrations of
122 solids were determined using an adaptation of EPA SW 846 Method 3050B. The mineral sample
123 (between 10 and 40 mg) was digested with three ml of HCl and 1 ml concentrated HNO_3 (trace
124 metal grade) in a Teflon bomb overnight followed by 110 °C for 3 hours in an oven. The sample
125 was filtered (Whatman #42) and diluted to 50 ml with deionized water, followed by analysis
126 using inductively coupled plasma spectroscopy (ICP-OES; Varian Vista Pro) or atomic
127 absorption spectroscopy with graphite furnace (Varian GTA100Z). All mineral assays were
128 performed in triplicate and replicates had standard deviations of 5% or less. The mineral-coated
129 sandstone contained 14.6 g V kg^{-1} and 111 g U kg^{-1}. In order to obtain a concentrated sample of
130 the U-bearing minerals for XRD, the fine mineral fraction was separated from the sand grains by
131 agitating and sonicating in deionized water; decanting, centrifuging and drying the separated fine
132 minerals. These were digested and analyzed as described above and characterized also by XRD
133 and SEM-EDS to identify the minerals.
134
135 **2.2 Culture experiments**
136 **2.2.1 Cultivation of CN32 with U and V as electron acceptors**
137 The cultures of *S. putrefaciens* CN32 that we used were originally isolated from the
138 Morrison Formation in New Mexico (Fredrickson et al., 1998). It is, therefore, a terrestrial rather
139 than a marine isolate and occurs in the same geological setting as the U-ore minerals. Cultures
140 were maintained as frozen stocks in our lab and were revived from frozen stock for each
141 experiment. The defined culture medium (DM)contained 10 mM sodium lactate and 1mM

142 phosphate , added as Na_2HPO_4, as previously described in Glasauer et al., 2003. Cultures reached
143 the stationary growth phase under oxic conditions after around 24 hours. For the incubation
144 experiments with the U-ore, 1.6 g of CGM-sandstone was added to 80 ml of minimal medium +
145 lactate in serum bottles, degassed with N_2, sealed and autoclaved. Bottles were inoculated in the
146 glove box (Coy; 3% H2/97% Ar) where they remained throughout the experiments. For the
147 treatments with soluble U and V, preparation and incubation conditions were identical, except U
148 and V were added from stock solutions prepared from uranyl acetate and sodium vanadate,
149 respectively. Final concentrations for U and V for these treatments were 1 mM each.
150 CN32 cultures were prepared for inoculation as previously described (Glasauer et al.,
151 2003). After conditioning the bacteria to grow on the defined medium (DM), the final pellet was
152 resuspended in DM to form a slurry of bacteria. The slurry was transferred to the glove box (no-
153 vacuum mode) and inoculated to achieve an initial concentration of around 10^8 cfu/ml,
154 determined by protein assay (Glasauer et al., 2001). All treatments were performed in triplicate.
155

156 **2.2.2 Growth inhibition assay**

157 For the growth inhibition assay, we selected conditions to model exposure of bacteria to
158 U(VI) and V(IV), the oxidation states of U and V that dominated in the incubation treatments
159 with CGM. Conditions were oxic to maintain the oxidation state of the metals and to facilitate the
160 assay procedures. A modified micro-dilution method (Wiegand et al. 2008) was used to assess
161 soluble U(VI) and V(IV) (0.001-1 mM) for microbial growth inhibition. In order to compare the
162 response of CN32 to *E. coli* K-12, a well characterized bacterial strain, bacteria were cultured in
163 one-tenth strength trypticase soy broth (10 % TSB) that has been shown to be compatible with
164 metal and mineral studies (French, 2013a; Hunter & Beveridge 2005). The volume was set to 200
165 µl/well. Stock solutions containing 0.02 M $UO_2(CH_3COOH)_2$, 0.1 M VCl_4, or 0.1 M $CaCl_2$ were

166 deoxygenated by bubbling oxygen-scrubbed N_2 gas (30 min/100 ml and 10 min for headspace
167 degassing). VCl_4 was prepared in HCl and solutions were pH-adjusted with NaOH. Degassed
168 solutions were transferred to an anaerobic chamber and sterilized by syringe filtration through a
169 sterile 0.22 µm filter into acid-washed autoclaved serum bottles. The stock solutions were
170 removed from the anaerobic chamber, stored in the dark, and visually inspected for precipitates,
171 flocs or colour change prior to use. Aliquots were aseptically removed from the stock solutions,
172 as required, using a syringe and fine gauge needle. *S. putrefaciens* CN32 and *E. coli* K-12 were
173 inoculated into 10 % TSB and grown for 16-20 h (room temperature, 60 rpm). 10 % TSB was
174 inoculated from these starter cultures at 15 % (vol/vol); stirred at 300 rpm (stir plate) at room
175 temperature (*S. putrefaciens* CN32) or 37 ºC (*E. coli* K-12), grown to an OD_{600} of 0.4-0.5 units
176 and adjusted to a final in-assay concentration of 5 x 10^5 CFU/ml. Negative growth control wells
177 contained sterile medium; positive growth control wells contained inoculated medium. The plates
178 were incubated for 20 h at optimum conditions (room temperature for *S. putrefaciens* CN32 or 37
179 ºC for *E. coli* K-12), then removed and observations on the presence/absence of visible growth
180 were recorded. The MIC was the lowest concentration which resulted in optically clear wells
181 denoting no cell growth. Assays were done as triplicate replicates and repeated as independent
182 duplicate experiments (n = 6).
183
184 **2.2.3 Biofilm formation assay**
185 The influence of soluble U(VI) and V(IV) (0.001-1 mM) on biofilm formation was
186 performed as for the growth inhibition assay except that the biofilms were grown on the inner
187 wall of sterile glass tubes which contained 2 ml volumes of 10% TSB with U, V or Ca added.
188 Following incubation for 20 h at room temperature (*S. putrefaciens* CN32) or 37 ºC (*E. coli* K-
189 12), the tubes were removed and 0.1 ml of Hucker's crystal violet was added. After 15 min

190 incubation (room temperature), the contents were gently decanted, excess unretained stain was
191 removed by washing with distilled water, and the tubes were air dried. Retained stain was
192 solubilized with 33% acetic acid and the absorbance (600 nm) was measured using a Bio-Tek
193 EL800 plate reader. Assays were done as triplicate replicates and repeated as independent
194 duplicate experiments (n = 6).
195
196 **2.3 Assessment for biotransformed elements**
197 **2.3.1 Electron microscopy**
198 Samples for transmission electron microscopy (TEM) were prepared as previously
199 described, for whole mount and thin section preparation (Glasauer et al., 2001). No metal stains
200 were used, so that all observed contrast was imparted to the bacteria by the metals (chiefly U and
201 V) present in the culture medium. Observations were made using a Philips CM10 TEM operating
202 at 80 kV, using an EDAX Sapphire detector and Genesis software. Scanning electron microscopy
203 was performed on untreated CGM-ore, and after 4 months incubation with CN32 on a Hitachi
204 S4500 field emission SEM. Secondary electron (SE) images were obtained with a 5 kV electron
205 beam. The samples were sputtered with gold to alleviate charging problems during SEM
206 examination.
207
208 **2.3.2 X-ray diffraction**
209 Biotransformation of the CGM appeared to have ceased by 10 months. At this time, the
210 mineral solids were separated into their component fractions, identified as the sand or fine
211 fraction. Separation was carried out in the glove box (3% H2/97% Ar). Suspensions were shaken
212 and the suspension bearing the fine clay fraction was decanted. This process was repeated until
213 the wash solution remained clear. All washes were combined in one centrifuge tube, which was

sealed, removed from the glove box, and centrifuged (5000 x g). The resulting pellet was dried in the glove box and lightly crushed with a mortar for analysis.

XRD data were acquired with a custom X-ray diffractometer at the Department of Physics, University of Guelph. The X-ray diffractograms were recorded from 5 to 80 °2Θ with a step width of 0.0125 °2 Θ and five seconds counting time. The applied Cu wavelength was created by a rotating anode. Analysis of the XRD data was carried with the help of the evaluation program EVA15.0 and LeBail (LeBail et al., 1988) with TOPAS4-2 by Bruker AXS.

2.3.3 Scanning Transmission X-ray Microscopy (STXM)

STXM analyses were conducted at the Molecular Environmental Science Beamline 11.0.2 (90 – 2000 eV) of the Advanced Light Source at Lawrence Berkeley National Laboratory (Bluhm et al. 2005). Culture samples were enclosed between a pair of 100 nm thick Si_3N_4 membranes. A micro-liter droplet of culture was deposited onto a Si_3N_4 window (Silson Ltd.), air-dried and then sandwiched with another window and hermetically sealed with glue. Another batch of treatments were analyzed in hydrated conditions using the same protocol, except the wet droplet was sandwiched immediately and the assembly sealed with glue. Uranium-bearing powder standards were deposited onto a Si_3N_4 window using a standard inspection microscope at 20x magnification. A 2 cm human hair fiber fixed to a tantalum wire was used to transfer the radioactive powder particles onto the window, then sandwiched and hermetically sealed with glue. Standards measured were $^{238}UO_2$ obtained from Alfa-Aesar, and mineral samples were obtained from Excalibur Mineral Corporation (New York). Small metal foil containers were inserted into the STXM prior to use with radioactive materials so that radioactive material could be captured in case of membrane failure.

STXM measurements were performed using a Fresnel zone plate lens (35nm outer zones)

to focus a monochromatic X-ray beam onto a 2D-scanned sample to record images in transmission mode using a scintillator-photomultiplier detector assembly. The imaging contrast is based on core electron excitation by X-ray absorption. X-ray images recorded at energies just below and at the relevant absorption edges were converted into optical density (OD) images and used to derive elemental maps. The optical density (OD) can be expressed for a given X-ray energy by the Beer-Lambert law as $OD=-\ln(I/Io)=\mu\rho t$ where I is the transmitted flux through the sample, I_0 is the incident flux, μ is the mass absorption coefficient, ρ is the density and t is the sample thickness. NEXAFS measurements were performed at the V 2p, O 1s and U 4f edges and obtained from image sequences (i.e., stacks) collected at energies spanning the relevant element absorption edges (508-555 eV at V 2p, O 1s edges; 715-800eV at U 4f edges, unless otherwise specified). A minimum of two different sample regions were analyzed for each element and two different batches of samples were analyzed. The STXM was pumped-purged with He to avoid decompressing the Si_3N_4 sandwiched samples. The theoretical spectral and spatial resolutions during our measurements were +/- 100 meV and 40 nm respectively. The photon energy was calibrated at the C 1s edge using the 3p Rydberg peak of gaseous CO_2 at 292.74 eV, at the O1s using the O 1s→3s transition at 538.9 eV of gaseous CO_2 and at the U 4f edges using gaseous Neon transition at 867.3eV. All data processing was carried out using IDL aXis2000 software (Hitchcock, 2019).

3.0 RESULTS

3.1 Characterization of the sandstone ore minerals

The U- and V- containing mineral components occurred as bright yellow coatings of fine basal plates (1-2 µm) on sand grains (grain size 200-500 µm) (Figure 1). The U-coated sandstone contained around 11 % U and 1.5 % V by weight. Based on the fit of the diffraction peaks, the

262 space group, and the chemical composition of the separated fine fraction (Table 1), we identified
263 the main minerals of the yellow solid as meta-tyuyamunite [$Ca(UO_2)_2(V_2O_8)\cdot 3H_2O$] and
264 fritzscheite [$Mn(UO_2)_2(V_2O_8)\cdot H_2O$] (Fitch and Murakami, 1999) (Figure 1). Both minerals are
265 members of CGM, which consist of uranyl divanadate layer complexes with interlayer cations.
266 The space group for both minerals is orthorhombic as confirmed by applying the LeBail method
267 (LeBail et al., 1988). Meta-tyuyamunite is a dehydrated variant of tyuyamunite and can
268 accommodate up to several percent structural K (Stern et al., 1956). Barium can substitute for Mn
269 in the interlayer of fritzscheite, but the structure does not accommodate K (Fitch and Murakami,
270 1999). Chemical analysis revealed that both Ba and Mn are present in the fine fraction of the
271 CGM ore (Table 1) as also confirmed by STXM (Appendix A).
272
273 **3.2 Microbial reduction of V and U**
274 Each incubation treatment with the CGM contained a total of 5 mM V and 7 mM U. Total
275 soluble V initially increased, followed by a decrease to a plateau at around 1 mM by 120 days
276 (Figure 2). The concentration of dissolved uranium was low throughout the incubation.
277 Vanadium III, IV, and V may be visually differentiated in solution by green, blue and
278 orange/yellow colors, respectively (Macara, 1980; Evans and White, 1987). The treatments that
279 contained the CGM ore and CN32 developed a blue-green color within one hour of inoculation.
280 Over time, the characteristic bright yellow color of the CGM disappeared. We observed the
281 development of three distinct layers in the culture bottles: clean sand grains at the bottom, a layer
282 of grey-green fine material, and clear blue liquid. Analysis for total U and V in the fine fraction
283 showed no change in U concentration after 10 months, and a slight decrease in V (Table 1). The
284 alkali elements Na and K were higher in the fine fraction after incubation, which likely reflects
285 the Na and K present in the culture medium. Calcium was significantly lower, Mg showed little

286 change, and Ba was slightly decreased in the post-reduction solids. The increase in K and
287 decrease in Ca of the solids is consistent with the observed transformation from tyuyamunite to
288 carnotite ($[K_2(UO_2)_2(V_2O_8)\cdot 3H_2O]$).

289 Bacteria were still viable after 5 months at a density of around 5 x 10^5 colony forming
290 units (cfu) ml^{-1}. The population reached a plateau around 10^5 cfu ml^{-1} that was maintained
291 between 6 d and at least 138 d. The cell density was around 10^3 cfu ml^{-1} after 8 months. Cell
292 numbers could be underestimated due to the tendency of the bacteria to form flocs; other methods
293 for determining cell numbers (i.e., fluorescent probes, light scattering) could not be used due to
294 the interference of the minerals with light. Bacteria were closely associated with the mineral
295 particles throughout the incubation (Figure 3). Over time, biofilms with cells embedded in a
296 matrix of exopolymeric substances (EPS) decreased in abundance, and bacteria were observed
297 mainly as single or few cells by four months (Figure 3 and Appendix B).

298 For comparison with the CGM treatments, we inoculated anoxic media containing
299 dissolved V(V) and U(VI) at 1 mM concentration each with CN32 cultures. These
300 concentrations are below the minimal inhibitory concentrations (MIC) of V(V) and U(VI) for *E.*
301 *coli,* a Gram-negative model bacterium (Nies, 2007); MIC data for CN32 is not available. The
302 cultures were monitored for V, U and cell concentrations for one week, at which point cell counts
303 had declined to less than 20 cfu ml^{-1} from an initial density after inoculation of around 10^8 cfu ml^{-1},
304 and no further chemical changes were observed. Vanadium reduction began within 20 minutes
305 of inoculation as shown by the rapid development of blue color in the medium and V in solution
306 stabilized at around 0.1 mM by 30 hours (Figure 2). The concentration of U in solution quickly
307 decreased and remained low; this decrease corresponded to the formation of a dark, fine grained
308 precipitate visible in the culture bottles. Uranium in solution also decreased rapidly in the

309 bacteria-free control, which corresponded to the appearance of white precipitates, likely uranium
310 phosphate minerals based on SEM imaging and EDS analysis (Appendix C).
311
312 **3.3 Changes in chemistry and mineralogy during incubation of carnotite group minerals**
313 Oxygen K-edge NEXAFS is an excellent probe for the covalency of actinide-oxide bonds
314 (Wu, 1999; Minasian et al., 2013; Wen et al., 2014). Initial STXM investigations of uranium
315 oxides have shown that the $4d_{5/2}$ edge is the most useful absorption edge for STXM in the soft X-
316 ray region above ~100 eV. In the case of uranium, this edge has a reproducible charge state shift
317 of ~1.3 eV from uranium (IV) dioxide to uranium (VI) trioxide (Kalkowski et al, 1987; Nilsson et
318 al, 2005). There have been several studies of metallic uranium compounds at the 4d edges
319 (Kalkowski, et al. 1987, Van der Laan 2004). A useful comparison is to the actinide metallic
320 counterparts of the dioxides at the $4d_{5/2}$ edge from these studies. The differences in band
321 structures for actinide metal versus actinide dioxide can lead to $4d_{5/2}$ edge peaks with different
322 widths. This has been observed in the NEXAFS of transition metals and transition metal oxides
323 (de Groot, 1991). For vanadium, the 2p ($L_{2,3}$) absorption spectra are useful to detect oxidation
324 states of V(V), V(IV) and V(III) (Cressy et al., 1993; Abbate, 1994; Maganas et al., 2014). Using
325 STXM, we identified V(V) and V(IV) during the incubation with the U-sandstone. In support of
326 our initial visual observations, V(IV) was detected 1 d after inoculation and was the dominant
327 oxidation state detected in association with the bacteria, although V(III) was also detected during
328 the 10 month period. Some V persisted as V(V) throughout, supporting that chemical
329 transformation of the U-bearing minerals was incomplete. In contrast, U was detected only as
330 U(VI) (Figure 4). Differences in the spatial distribution of U and V developed over time, as
331 observed on regions of the solid material (Figure 5), and which is consistent with the detection of

V(IV). Fine precipitates formed that appeared to coat larger mineral grains and bacteria (Figure 3d).

The concentration of Fe was relatively low in the fine fractions (Table 1). The iron valency appeared to be stable as Fe(III) throughout the incubation; STXM analysis showed areas of high Fe concentration as particulates. We also examined the sand fraction and fine fractions that formed distinct layers during the incubation using XRD. The sand fraction contained quartz, with traces of cristobalite and feldspar (sanidine) (Figure 1). In the fine fraction, refinement of the data indicated a mixture of K-carnotite, which belongs to the monoclinic space group, and meta-tyuyamunite. This fraction was enriched in K and depleted in Ca compared to the initial yellow fine fraction (Table 1), consistent with the appearance of carnotite. Fritzscheite was not detected even though Mn and Ba concentrations in the fine fraction were relatively unchanged after incubation (Table 1). Observations using SEM showed mineral particles that had a platey structure similar to that seen for the initial U-bearing minerals, but the plates were thinner and formed rosettes (Appendix C). SEM-EDS indicated elevated concentrations of P in association with U for these structures, suggesting autunite [$Ca(UO_2)_2(PO_4)_2 \cdot 10\text{-}12(H_2O)$], which can also accommodate Na and K. Autunite could not be confirmed by bulk XRD likely because of very low abundance, but it is supported by STXM results (Figure 4). Distinct particles of vanadium oxide (VO_2) were observed in association with the bacteria by STXM (discussed below) but were also not detected by bulk XRD. There was no chemical, mineralogical, or visual evidence for a distinct UO_2 component.

3.4 Associations between bacteria, U and V

3.4.1 Carnotite group mineral ore

355 STXM images show the bacteria were closely associated with nm and micron-sized
356 particles of the CGM. (Figure 5). Wet samples imaged using STXM after one week revealed
357 bacteria embedded in an extensive exopolymer matrix that contained protein, lipids, and
358 polysaccharides , consistent with biofilm formation and growth, with distinct mineral particles
359 distributed heterogeneously within the biofilm matrix (Appendix B). Over time, the bacteria
360 appeared to associate preferentially as individuals or as clusters of few cells with the CGM.
361 Sparse, fine (2-3 nm) precipitates accumulated on the bacteria (Figure 3d). We did not observe U
362 or V precipitates in the periplasm or cytoplasm of CN32 during the incubation of CGM, as
363 assessed by TEM observations on thin sections. This supports that metal reduction took place
364 outside the cell, consistent with the location of metal reducing enzymes at the outer leaflet of the
365 outer membrane (Myers and Myers, 1992).
366 Elemental maps of the solid phase after 8 months show the close correspondence between
367 V, U, Ba, Ca and K (Appendix A).
368
369 **3.4.2 Soluble U and V**
370 After inoculation with CN32, the medium became light blue within two hours, indicating
371 reduction of V(V) to V(IV). Fine precipitates accumulated in the periplasm of the bacteria and
372 external to the cell during the incubation, as observed by TEM on thin sections and reported by
373 others for dissimilatory U(VI) reduction (e.g., Lloyd et al., 2002). Bacteria formed flocs
374 containing an abundant matrix of exopolymeric substances (EPS) during reducing conditions.
375 The EPS contained proteins, lipids and carbohydrates, and is chemically similar to the biofilms
376 observed for the CGM treatment, as indicated by STXM (data not shown). Uranium and
377 vanadium appeared to concentrate in the extracellular matrix (Figure 6). After 24 hours, we

detected U(IV) and V(III) within the matrix of bacteria, exopolymer and mineral solids. Uranium (VI), V(V) and V(IV) were not detected after 24 hours (Figure 6).

3.5 Growth inhibition and biofilm assays

Because of the longevity of CN32 in the U-ore treatments compared to those with soluble U and V, we tested growth inhibition over a range of U(VI) and V(IV) concentrations. Vanadyl [V(IV)] was included rather than V(V) because it was the form of V present in association with bacteria during the incubation with the U-ore, whereas U(VI) was the only observed oxidation state of U in the same treatment. Vanadyl is stable in solution against oxidation for at least 24 hours (French et al., 2013a). To maintain these oxidation states of U and V, the assays were conducted under aerobic conditions, with the understanding that CN32 adjusts cell wall biochemistry in response to oxygen presence (French et al., 2013a). The results should, therefore, be interpreted qualitatively and to compare relative responses to different metal concentrations. *Escherichia coli*, well studied as a model Gram-negative organism, was included as a reference strain (K-12). Calcium was included as a cation which, at the tested concentrations, would not have negative impact on cell growth. Calcium ions have important roles in maintaining cell wall health and affect fundamental processes such as bacterial adhesion (Ilangovan et al., 2001; Naik et al., 2006). Calcium and V(IV) did not inhibit growth at any of the tested concentrations, for both bacterial species. *S. putrefaciens* was 100-fold more sensitive to the presence of U(VI) than was *E. coli*, with growth suppressed at concentrations of 0.01 and 1 mM respectively. *E. coli* strains in general have shown tolerance to a wide range of metals (Nies, 2007).

The influence of these soluble metals on the formation and growth of biofilms was also investigated. As noted earlier, cells surrounded by EPS were intimately associated with the carnotite group minerals or occurred as flocs following incubation with U and V species; both are

consistent with descriptions of bacterial growth as a biofilm. To assess biofilm development in the presence of dissolved V and U, biofilms were assessed as staining of biomass attached to glass test tubes, shown by the band thickness and density (Figure 7). Dense biofilms were formed at all concentrations tested of Ca and V for CN32, but only at the lowest concentration of U, 0.001 mM. At this concentration, the amount of biofilm was increased by 30% relative to the control. The stimulation of biofilm growth by sub-inhibitory concentrations of U is reminiscent of bacterial responses to environmental stresses such as sub-inhibitory concentrations of antibiotics (Andersson and Hughes, 2014). In contrast, *E. coli* did not show increased biofilm formation in response to sub-inhibitory U(VI) and formed less abundant biofilms overall (Figure 7). The outer membrane of *S. putrefaciens* is known to be perturbed by uranium (French, 2013a), with the possible induction of stress responses (reviewed in Kolhe et al., 2018). Vanadium stimulated biofilm growth of *S. putrefaciens* at 1 mM only, with values increasing by 60 % relative to the control; lower concentrations of V yielded values similar to the control. Calcium had little impact on biofilm growth.

4.0 DISCUSSION

4.1 U and V chemical transformations

The reduction of naturally occurring, solid phase U(VI) has been demonstrated to date only for U(VI) precipitates located between larger lithic fragments (Liu et al., 2009). We did not observe a net chemical reduction of U(VI) in CGM, in agreement with other studies that did not observe U(VI) reduction when different U-containing minerals were incubated with metal reducing bacteria (Ilton et al. 2006; Smeaton et al. 2008). This outcome is likely due to steric and bonding considerations (Stohl and Smith, 1981), similar to limits on Fe reduction observed under nutrient limited conditions (Glasauer et al., 2003).

426 In contrast to U(VI), a portion of the V(V) in the CGM was readily reduced. Based on
427 half-cell reduction potentials, V(V) in pure solution under standard conditions can be expected to
428 reduce to V(IV) more readily than Fe(III)→Fe(II) or U(VI)→U(IV) (Lee, 1992). The chemical
429 form of the metal and the chemical conditions will clearly impact reducibility (Cumberland et al.,
430 2016). The reduction potentials for U or V contained in CGM is unknown. In addition, the ore
431 that we used contained at least two distinct uranyl vanadate minerals, meta-tyuyamunite and
432 fritzscheite, and it was not possible to observe their behavior separately during the incubation. It
433 is likely that the minerals were not chemically pure due to element substitutions and traces of
434 other associated elements.
435 The presence of V(III) species observed during reduction of the CGM stands in contrast to
436 the lack of U(VI) reduction; V(III) indicates strongly reducing conditions (Wehrli and Stumm,
437 1989). In a related study, V(III) was not detected in the bulk solution when CGM was incubated
438 with CN32 under identical culture conditions, although V(III) was observed during the
439 dissimilatory reduction of V(V) added as a sodium vanadate salt (Li et al., 2007). Although the
440 STXM results present a consistent picture of U and V chemistry during the incubation, it is
441 feasible that local areas may have contained U(IV) that was below detection limits or was not
442 examined. In contrast, U(IV) was detected consistently in the treatments with soluble V(V) and
443 U(VI) using STXM (Figure 6). V(III) was also detected (Appendix D); however, we cannot rule
444 out beam-induced damage on this dataset. Overall, these data suggestmore highly reduced
445 conditions.
446 The geochemistry of vanadium is particularly complex. Vanadium exists in multiple states
447 of oxidation, hydrolysis, and polymerization (Macara, 1980; Huang et al., 2015). Pentavalent
448 species are especially prone to polymerize; at concentrations as low as 1 mM and neutral pH,
449 HVO_4^{2-} aggregates into trimers and tetramers. Vanadate species, similar in chemical behavior to

phosphate, readily form polynuclear complexes with phosphate as well as surface complexes with hydrous oxides (Wehrli and Stumm, 1989). The redox transition for V(V)-V(IV) occurs at E_H values comparable to those for Mn(II)-Mn(IV), around 0.1 – 0.5 V, which is characteristic for sediment-water interfaces (Wehrli and Stumm, 1989). Vanadyl species in many natural waters are predicted to hydrolyze, sorb strongly to mineral surfaces, and are considered relatively insoluble (Wehrli and Stumm, 1989; Huang et al., 2015). The gradual disappearance of total V from solution correlates with the accumulation of V(IV) and V(III) precipitates observed on the bacteria, likely as $VO(OH)_2$ and V_2O_3. Vanadium(III) species are highly insoluble except in acidic conditions (below pH 2) and in the absence of O_2 (Macara, 1980).

4.2 Mineral Transformations

The minerals in the U-sandstone were transformed by two main processes: 1) bacterial dissimilatory reduction of V(V), and 2) exchange of cations contained in the interlayer of the carnotite group minerals. The incubation studies with CGM illustrate how biotic and abiotic processes can simultaneously affect mineral transformation. Given that U(VI) and V(V) only coexist in mineral form when both are oxidized (Langmuir, 1978), the bacterial reduction of V(V) would necessarily release both metals. The separation of V and U consequent to V reduction is supported by the appearance of V oxide particles on the bacteria and the appearance of distinct solids containing U and P. Soluble U was not detected during the transformation of CGM. The high affinity of U for adsorption to organic matter and minerals would scavenge dissolved U, which could help foster the precipitation of U phases. Precipitates of fine-grained V- and U-containing phases that formed during the incubation could only be indirectly assessed for mineral properties, i.e., using SEM, TEM and STXM. These nanometer-scale particles can be directly

linked to the microbial transformation of V(V) contained in the U-sandstone minerals. STXM elemental maps revealed regions where U appeared to be distinct from V, suggesting separation.

Mineral formation was likely fostered by the controlled conditions of our experiments, e.g., the concentration of K in the culture medium likely favored CGM over fritzscheite. The limits to cation substitution for the interlayer of the UO_2VO_4 sheets have not been established. The elements that comprise the distinct variants include K, Pb, Ba, Mn, Cs, Ca, Cu, Na, and Al (no Fe variant is known) (Finch and Murakami, 1999), although it is feasible that additional substituted cations could occur in low concentrations. In addition, structural water in the interlayer can vary. For example, hydration-dehydration for tyuyamunite is reversible for water contents ranging from 3-8.5 H_2O, with meta-tyuyamunite at the lower end of that range. (Stern et al.1956). The optical properties and XRD patterns of the CGM variants are distinct, analogous to the behavior of swelling clays such as montmorillonite that respond similarly to hydration or exposure to cations having different radii. Although these transformations were a consequence of experimental conditions, they illustrate the flexible response of the minerals to changes in their chemical surroundings, on short time scales, which can have implications for mineral solubility. For example, carnotite is less soluble than tyuyamunite under some conditions (Hostetler and Garrels, 1962, Weeks, 1961). Carnotite group members typically occur together in complex assemblages which cannot be physically separated and respond readily to environmental conditions (Stern et al., 1956, Finch and Murakami, 1999).

In addition, the microscopy studies – both SEM and STXM – support that autunite formed during the incubation, suggesting that U(VI) that was released from the U-ore minerals was immobilized by precipitation with phosphate.

4.3 Reactions at bacteria-mineral and bacteria-metal interfaces

497 The lack of periplasmic precipitates during the dissimilatory reduction of V in CGM
498 supports that reduction took place at the interface between the cell wall and the extracellular
499 environment. For Gram negative bacteria, the outer and plasma membranes sandwich the
500 periplasm, a gel-like region that contains proteins involved in shuttling chemicals and electrons
501 between the outer membrane and the cytoplasm. Shuttling factors include soluble cytochrome
502 proteins that can reduce soluble, oxic forms of metals during anaerobic respiration. If the reduced
503 form of the metal is insoluble, nano-sized precipitates form in the periplasm, as documented for U
504 and Tc (e.g., Lloyd et al., 2002) and observed during the reduction of soluble V and U in our
505 treatments.
506 It is unknown how bacteria that respire metals maintain critical chemical gradients and
507 membrane fluidity, and continue to uptake nutrients, when bulk conditions favor the sorption of
508 metals and minerals to the cell envelope (French et al., 2013b). Bacteria are highly interactive
509 with dissolved metal ions due to a high surface-to-volume ratio and a high density of metal-
510 reactive functional groups in the cell wall (Beveridge, 1989). They develop extracellular
511 gradients by actively and passively taking up and expelling metals and other chemical species. As
512 a result, the interface between the cell wall and the immediate extracellular environment differs in
513 metal composition and concentration from the bulk suspending fluid. Metal speciation is also a
514 factor; for example, the rate of Fe^{3+} reduction has been shown to depend on the form of the metal
515 that is present: soluble, complexed, sorbed or mineral (Urrutia et al., 1998; Zachara et al., 1998;
516 Haas and DiChristina, 2002; Glasauer et al., 2003). Cell respiration may contribute to keeping
517 metals in solution near bacteria through H^+ efflux. For example, more acidic pH values were
518 observed proximal to bacteria in a biofilm, relative to the bulk exopolymer, which was suggested
519 to increase metal solubility (Hunter and Beveridge, 2005). Bacteria have biochemical responses
520 to environmental change that may help them resist the impacts of soluble metals on the cell wall.

In earlier research, we observed that *S. putrefaciens* CN32 altered lipid chemistry in response to uranium and vanadium, as well as in response to oxygen, which may impact the accumulation of these elements (French et al., 2013a). In the case of the treatments with soluble U and V, the accumulation of these elements in the exopolymer matrix and their exclusion from the bacteria suggest distinct microenvironments, although this remains speculative.

Our results support that biofilms and flocs of CN32 immobilize U, as shown by others for U in the presence of microbes in controlled studies (reviewed in Cao et al., 2011; Cologgi, 2014; Stylo et al, 2015). Immobilization has been demonstrated in a field study of natural biofilms (Amano et al., 2017) and in natural organic matter associated with surface and subsurface sediments (Bone et al., 2017; Bone et al., 2020). In particular, Cao et al. (2011) showed that adsorption of U(VI) is competitive between EPS and cells of *Shewanella* HRCR-1, with a higher proportion of U(VI) associated with EPS when U(VI) concentrations were lower. This study (Cao et al., 2011) also showed that the presence of EPS did not affect the reduction efficiency of U(VI) to U(IV), with around 60% of U(VI) reduced at a concentration of 1 mM, identical to the concentration we used to investigate reduction of soluble U(VI) and V(V). Microorganisms respond to environmental stresses such as nutrient limitation as well as to antimicrobial stress by producing EPS (e.g., Myska and Czaczyk, 2009; Andersson and Hughes, 2014). The response of CN32, in terms of growth and proliferation of exopolymeric substances (EPS), may enhance survival by keeping U species from interacting with membrane lipids, which decreases membrane fluidity (French et al., 2013a). The role of EPS in binding potentially toxic elements is not well understood, largely due to differences in methodology (reviewed in Butzen and Fein, 2019). We speculate that the binding of U to high affinity sites in EPS, as observed for Cd (Butzen and Fein, 2019), would favor bacterial survival. We cannot, however, infer that the response of CN32 to the lowest concentration of U in our study of biofilm formation is unequivocally a defense

545 mechanism. It is nevertheless remarkable that CN32 responds in a way that appears to keep U
546 away from the cell wall. Our observation that this occurs particularly at sub-inhibitory
547 concentrations of U suggests that EPS formation and reduced toxicity are linked. A link between
548 EPS and reduced toxicity to bacteria may also help to explain why the response to V occurred
549 only at much higher concentrations, given the relatively low toxicity of V.
550 A change from oxidizing to reducing conditions, such as at redox transition zones, may
551 mobilize V in the short term from carnotite-type minerals. Uranium (VI) species that are released
552 consequently will sorb to minerals and precipitate at low ion activity; however, it should be kept
553 in mind that the affinity of U species for organic matter is particularly high (reviewed in
554 Cumberland et al., 2016). In one study, this affinity had a greater impact on U mobility than did
555 complexation by carbonate species, despite thermodynamic predictions (Yang et al, 2012). In our
556 studies, U did not become soluble when the CGM were transformed under reducing conditions,
557 indicated by the lack of U in solution or associated with cells in this treatment. If V and U remain
558 in pore water and adsorbed to solids, a return to oxidizing conditions could induce the
559 precipitation of uranyl vanadate minerals (Tokunaga et al., 2009; Tokunaga et al., 2012). The
560 strong interaction of U(VI) with organic matter is speculated to have immobilized and
561 concentrated U in the Colorado Plateau environment (Cumberland et al., 2016; Spirakis, 1996;
562 Hansley and Spirakis, 1992) with eventual precipitation.
563
564 **4.4 Implications for ore formation**
565 The formation of carnotite-type deposits is controversial. In the Colorado Plateau, it has
566 been hypothesized that cycles of reducing and oxidizing conditions have created the present roll
567 front and tabular structures that characterize the deposits (Weeks,1961; Hostetler and Garrels,
568 1962). V(III) and U(IV) existing separately in primary reduced minerals would have mobilized

upon exposure to moderately oxidizing conditions in weathering environments. Transport as U(VI) and V(IV) species under slightly reducing (-0.1 V), alkaline conditions is one proposed scenario (Evans and Garrels, 1958; Weeks, 1961). These redox conditions are similar to those created during the anoxic incubation of CN32 with the CGM. It is likely that U and V were transformed during cycles of oxidizing and reducing conditions; reducing conditions would have prevailed, for example, in the organic-rich Triassic deposits which may have been infiltrated by U-bearing fluids during the Jurassic period (Hansley and Spirakis, 1992; Spirakis, 1996). Subsequent oxidizing conditions would have led to the mobilization and ultimate coprecipitation of V and U as carnotite-type minerals. Bacterial activity may continue to exert an important control on the mobility of both U and V in the subsurface environment of the Colorado Plateau today.

5.0 CONCLUSIONS

Our results support previous studies in demonstrating the resistance of mineral U(VI) to bacterial reduction. In contrast to those studies, however, the carnotite group minerals include an alternate oxidized element, V(V), that readily served as an electron acceptor in our experiments. Reduction of mineral-bound V(V) did not liberate U into solution; instead, there was evidence that autunite was formed. The initial carnotite group mineral fritzscheite was transformed to K-carnotite through the replacement of interlayer cations, indicating that mineral changes were induced through biotic and abiotic pathways. In contrast to our investigations with mineral U and V, soluble V(V) and U(VI) were readily reduced in the presence of metal-respiring bacteria. The abundant exopolymer matrix which surrounded the bacteria during respiration of the soluble electron acceptors appeared to accumulate these elements in preference to bacterial surfaces. This

suggests that the biofilm matrix helped to reduce the exposure of bacteria in particular to U, which is highly toxic. Understanding the role of biofilms in ameliorating toxicity is important given that exopolymeric substances are produced by bacteria in response to environmental conditions.

Natural environments contain many possible electron acceptors for bacteria that can adapt readily to challenging conditions. Understanding the relative availability of electron acceptors from the microbial perspective is key to interpreting element solubility and mineral transformation reactions in the present – and perhaps in the past.

6.0 AKNOWLEDGEMENTS

The authors are grateful to Brian S. Fairchild of LBNL EH&S for his help with the STXM experiments. We thank Farhana Islam and Christine Cousins for assistance with the culture experiments at the University of Guelph and Dr. Susan Koval (University of Western Ontario: London, ON, Canada) for provision of *Escherichia coli* K-12 (AB264 lineage). This research was supported by the Natural Science and Engineering Research Council (NSERC) through a Discovery grant to S. Glasauer. Parts of this research, the ALS, and the ALS-MES Beamline 11.0.2 were supported by the Director, Office of Science, Office of Basic Energy Sciences, Division of Chemical Sciences, Geosciences, and Biosciences and Materials Sciences Division of the U.S. Department of Energy at the Lawrence Berkeley National Laboratory under Contract No. DE-AC02-05CH11231 (SF, DKS, TT).

None of the authors has a competing interest for this research.

REFERENCES

Abbate M (1994). The O 1s and V 2p X-ray absorption spectra of vanadium oxides. Braz. J. Phys. 24: 785-795.

Amano Y, Iwatsuki T, Naganuma T (2017) Characteristics of naturally grown biofilms in deep groundwaters and their heavy metal sorption property in a deep subsurface environment. *Geomicrobiol. J.* 34: 769-783.

Andersson DI, Hughes D (2014) Microbiological effects of sublethal levels of antibiotics. *Nat. Rev. Microbiol.* 12: 465-478.

Anderson RT, Vrionis HA, Ortiz-Bernad I, Resch CT, Long PE, Dayvault R, Karp K, Marutzky S, Metzler DR, Peacock A, White, DC, Lowe M, Lovely DR (2003) Stimulating the in situ activity of Geobacter species to remove uranium from the groundwater of a uranium-contaminated aquifer. *Appl. Environ. Microbiol.* 69: 5884-5891.

Bargar JR, Williams KH, Campbell KM, Long PE, Stubbs JE, Suvorova EI, Lezama-Pacheco JS, Alessi DS, Stylo M, Webb SM, Davis JA, Giammar DE, Blue LY, Bernier-Latmani R (2013) Uranium redox transition pathways in acetate-amended sediments. *Proc. Natl. Acad. Sci* 110: 4506-4511.

Beveridge TJ (1989). Metal ions and bacteria. In Metal Ions and Bacteria, TJ Beveridge and RJ Doyle, eds. John Wiley and Sons, New York.

Bluhm H., Andersson K., Araki T., Benzerara K., Brown G.E., Dynes J.J., Ghosal S., Gilles M.K., Hansen H.-Ch., Hemminger J.C., Hitchcock A.P., Ketteler G., Kilcoyne A.L.D., Kneedler E., Lawrence J.R., Leppard G.G., Majzlam J., Mun B.S., Myneni S.C.B., Nilsson A., Ogasawara H., Ogletree D.F., Pecher K., Salmeron M., Shuh D.K., Tonner B., Tyliszczak T., Warwick T., Yoon T.H. (2006). Soft X-ray microscopy and spectroscopy at the molecular environmental science beamline at the Advanced Light Source, *J. of Electron Spectroscopy and Related Phenomena*:150: 86-104

Bone SE, Cahill MR, Jones ME, Fendorf S, Davis KHW, Bargar JR (2017). Oxidative uranium release from anoxic sediments under diffusion-limited conditions. *Environ. Sci. Tech.* 51: 11039-11047.

Bone SE, Cliff J, Weaver K, Takacs CJ, Roycroft S, Fendorf S, Bargar JR (2020). Complexation by organic matter controls uranium mobility in anoxic sediments. *Environ. Sci. Tech.* 54: 1493-1502.

Butzen ML and Fein JB (2019) Influence of extracellular polymeric substances on the adsorption of cadmium onto three bacterial species. *Geomicrobiol. J.* 36: 412-422.

660 Carpentier W, Sandra K, De Smet I, Brigé A, De Smet L and Van Beeumen J (2003) Microbial
661 reduction and precipitation of vanadium by Shewanella oneidensis. *Appl. Environ. Microbiol.* 69:
662 3636-3639.
663
664 Carpentier W, De Smet ., Van Beumen and Brigé A. (2005) Respiration and growth of
665 Shewanella oneidensis MR-1 using vanadate as the sole electron acceptor. *J. Bacteriol*. 187:
666 3293-3301.
667
668 Cao B, Ahmed B, Kennedy DW, Wang Z, Shi L, Marshall MJ, Fredrickson JK, Isern NG, Majors
669 PD, Beyenal H (2011) Contribution of extracellular polymeric substances from Shewanella sp.
670 HRCR-1 biofilms to U(VI) immobilization. *Environ. Sci. Technol*. 45: 5483-5490.
671
672 Cologgi DL, Speers AM, Bullard BA, Kelly SD, Reguera G (2014) Enhanced uranium
673 immobilization and reduction by Geobacter sulfurreducens biofilms. *Appl. Environ. Microbiol.*
674 80: 6638-6646.
675
676 Cressey G, Henderson CMB, van der Laan G (1993) Use of L-edge X-ray absorption
677 spectroscopy to characterize multiple valence states of 3d transition metals; a new probe for
678 mineralogical and geochemical research. Phys. Chem. Minerals 20:111-119.
679
680 Cumberland SA, Douglas G, Grice K, Moreau JW (2016) Uranium mobility in organic matter-
681 rich sediments: A review of geological and geochemical processes. *Earth-Science Reviews* 159:
682 160-185.
683
684 de Groot, FMF (1991) Ph.D. Thesis, X-ray Absorption of Transition Metal Oxides, University of
685 Nijmegen, Nijmegen, Netherlands
686
687 DiChristina TJ, Fredrickson JK and Zachara J. (2005) Enzymology of electron transport: Energy
688 generation with geochemical consequences; Reviews in Mineralogy and Geochemistry vol. 59
689 (eds. J. F. Banfield, J. Cervini-Silva and K. M. Nealson), pp. 27-52. Mineralogical Society of
690 America, Washington, D.C.
691
692 Eckstrom A, Fooks CJ., Hambley T, Loeh HJ, Miller SA and Taylor JC (1983) Determination of
693 the crystal structure of a porphyrin isolated from oil shale. *Nature* 306: 173-174.
694
695 Evans HT and Garrels R. (1958) Thermodynamic equilibria of vanadium in aqueous systems as
696 applied to the interpretation of the Colorado Plateau ore deposits. *Geochim. Cosmochim. Acta* 15:
697 131-149.
698
699 Evans HT and White JS (1987) The colorful vanadium minerals: A brief review and a new
700 classification. *The Mineralogical Record* 18: 333-340.
701
702 Finch R and Murakami T (1999) Systematics and paragenesis of uranium minerals. In Uranium:
703 Mineralogy, Geochemistry and the Environment; Reviews in Mineralogy vol. 38 (eds. P. C.
704 Burns and R. Finch), pp. 91-180.
705

706 Fredrickson JK, Zachara JM, Kennedy DW, Dong H, Onstott TC, Hinman NW, Li S (1998)
707 Biogenic iron mineralization accompanying the dissimilatory reduction of hydrous ferric oxide by
708 a groundwater bacterium. *Geochim. Cosmochim. Acta* 62, 3239-3257.
709
710 Fredrickson JK, Zachara JM, Kennedy DW, Duff MC, Gorby YA, Li S-M, Krupka KM (2000)
711 Reduction of U(VI) in goethite suspensions by a dissimilatory metal-reducing bacterium.
712 *Geochim. Cosmochim. Acta* 64: 3085-3098.
713
714 French S, Fakra S, Trevors ., Glasauer S (2013a) Changes in *Shewanella putrefaciens* CN32
715 membrane lipid chemistry and fluidity in the presence of soluble Mn(II), V(IV), and U(VI).
716 *Geomicrobiology Journal* 30: 245-254.
717
718 French S, Puddephatt D, Habash M, Glasauer S (2013b) The dynamic nature of bacterial
719 surfaces: Implications for metal-membrane interaction. *Critical Reviews in Microbiology* 39: 196-
720 217.
721
722 Glasauer S, Langley S, Beveridge TJ (2001) Sorption of Fe(hydr)oxides to the surface of
723 Shewanella putrefaciens: cell-bound fine-grained minerals are not always formed de novo.
724 *Applied and Environmental Microbiology* 67: 5544-5550.
725
726 Glasauer S, Weidler PG, Langley S, Beveridge T J (2003) Controls on Fe reduction and mineral
727 formation by a subsurface bacterium. *Geochim. Cosmochim. Acta* 67: 1277-1288.
728
729 Haas JR and DiChristina TJ (2002) Effects of Fe(III) chemical speciation on dissimilatory Fe(III)
730 reduction by *Shewanella putrefaciens. Environ. Sci. Technol*. 36: 373-380.
731
732 Hansley PL, Spirakis CS. 1992. Organic-matter diagenesis as the key to a unifying theory for the
733 genesis of tabular uranium-vanadium deposits in the Morrison Formation, Colorado Plateau.
734 *Economic Geology* 87: 352-365.
735
736 Hao L, Zhang B, Feng C, Zhang Z, Lei Z, Shimizu K, Xuelong C, Liu H, Liu H (2018) Microbial
737 vanadium (V) reduction in groundwater with different soils from vanadium ore mining areas.
738 Chemosphere 202: 272-279.
739
740 Hitchcock A. 2019. An IDL-based analytical package. http://unicorn.mcmaster.ca
741
742 Huang JH, Huang F, Evans L, Glasauer S (2015) Vanadium: Global (bio)geochemistry. *Chemical*
743 *Geology* 417: 68-89.
744
745 Hunter RC and Beveridge TJ (2005) Application of a pH-sensitive fluoroprobe (C-SNARF-4) for
746 pH microenvironment analysis in *Pseudomonas aeruginosa* biofilms. (2005) *Appl. Environ.*
747 *Microbiol.* 71: 2501-2510.
748
749 Hostetler PB, Garrels RM. 1962. Transportation and precipitation of uranium and vanadium at
750 low termperatures with special reference to sandstone-type uranium deposits. *Economic Geology*
751 57: 137-167.
752

753 Ilangovan U, Ton-That H, Iwahara J, Schneewind O, Clubb RT (2001) Structure of sortase, the
754 transpeptidase that anchors proteins to the cell wall of Staphylococcus aureus. *Proc. Natl. Acad.*
755 *Sci.* 98: 6056-6061.
756
757 Ilton ES, Liu C, Yantasee W, Wang Z., Moore DA, Felmy AR, Zachara JM (2006) The
758 dissolution of synthetic Na-boltwoodite in sodium carbonate solutions *Geochimica et*
759 *Cosmochimica Acta* 70: 4836-4849.
760
761 Kalkowski G, Kaindl G, Brewer W D, Krone W (1987) Near edge X-ray absorption fine structure
762 in uranium minerals. *Phys Rev B* 35:2667-2677
763
764 Khijniak TV, Slobodkin A, Coker V, Renshaw JC, Livens FR, Bonch-Osmolovskaya EA,
765 Birkeland NK, Medvedeva-Lyalikova NN, Lloyd JR (2005) Reduction of uranium (VI)
766 phosphate during growth of the thermophilic bacterium Thermoterrabacterium ferrireducens.
767 *Appl. Environ. Microbiol.* 71: 6423-6426.
768
769 Kolhe N, Zinjarde S, Acharya C (2018) Responses exhibited by various microbial groups relevant
770 to uranium exposure. *Biotechnology Advances* 36: 1828-1846.
771
772 Langmuir D. (1978) Uranium solution-mineral equilibria at low temperatures with applications to
773 sedimentary ore deposits. *Geochim. Cosmochim. Acta* 42: 547-569.
774
775 Le Bail A., Duroy H, Fourquet J. (1988). Ab-initio structure determination of $LiSbWO_6$ by
776 X-ray powder diffraction. *Math. Res. Bull*. 23: 447-452.
777
778 Lee J. D. (1992) Concise Inorganic Chemistry, 4th ed. Chapman and Hall, London.
779
780 Li L, Steefel CI, Kowalsky MB, Englert ., Hubbard SS (2010) Effects of physical and
781 geochemical heterogeneities on mineral transformation and biomass accumulation during
782 biostimulation experiments at Rifle, Colorado. *J. Contam. Hydrol.* 112: 45-63.
783
784 Li XS, Glasauer S, Le XC (2007) Speciation of vanadium in oilsand coke and bacterial culture
785 by high performance liquid chromatography inductively coupled plasma mass spectrometry.
786 *Analytica Chimica Acta* 602: 17-22 and 648: 128 (2009)
787
788 Liu C, Byong-Hun J, Zachara JM, Zheming W, Dohnalkova A and Fredrickson JK (2006)
789 Kinetics of microbial reduction of solid phase U(VI). *Environ. Sci. Technol*. 40: 6290-6296.
790
791 Liu C, Zachara JM, Zhong L, Heald SM, Wang Z, Byong-Hun J and Fredrickson JK (2009)
792 Microbial reduction of intragrain U(VI) in contaminated sediment. *Environ. Sci. Technol*. 43:
793 4928-4933.
794
795 Lloyd JR, Chesnes J, Glasauer S, Bunker DJ, Livens FR and Lovley DR (2002) Reduction of
796 actinides and fission products by Fe(III)-reducing bacteria. *Geomicrobiol. J.* 19: 103-120.
797

798 Lloyd JR and Renshaw JC (2005) Bioremediation of radioactive waste: radionuclide-microbe
799 interactions in laboratory and field-scale studies. *Current Opinion in Biotechnology* 16: 254-260.
800
801 Lovley DR, Phillips EJP, Gorby YA, Landa ER (1991) Microbial reduction of uranium. *Nature*
802 350: 413-416.
803
804 Lyalikova NN and Yurkova NA (1992) Role of microorganisms in vanadium concentration and
805 dispersion. *Geomicrobiology Journal* 10: 15-26.
806
807 Macara IG (1980) Vanadium – an element in search of a role. *Trends in Biochemical Sciences* 5:
808 92-94.
809
810 Maganas D, Moemelt M, Weyhermuller T, Blume R, Havecker M, Knop-Gericke A, DeBeer S,
811 Schlogl R, Neese F. 2014. L-edge X-ray absorption study of mononuclear vanadium complexes
812 and spectral predictions using a restricted open shell configuration interaction ansatz. Phys.
813 Chem. Chem. Phys. 16: 264-276.
814
815 Minasian SG, Keith JM, Batista ER, Boland KS, Bradley JA, Daly SR, Sokaras D, Kozimor SA,
816 Lukens WW, Martin RL, Nordlund D, Seidler GT, Shuh DK, Tyliszczak T, Wagner G, Weng T-
817 C, Yang P. (2013) Covalency in metal-oxygen multiple bonds evaluated K-edge spectroscopy
818 and electronic structure theory. *J. Amer. Chem. Soc.* 135, 1864-1871 (2013). DOI:
819 10.1021/ja310223b
820
821 Moskalyk RR and Alfantazi AM (2003) Processing of vanadium: a review. *Minerals*
822 *Engineering* 16: 793-805.
823
824 Myers CR and Myers JM (1992) Localization of cytochromes to the outer membrane of
825 anaerobically grown Shewanella putrefaciens MR-1. *Journal of Bacteriology* 174: 3429-3438.
826
827 Myszka K, Czaczky K (2009) Characterization of adhesive exopolysaccaride (EPS) produced by
828 Pseudomonas aeruginosa under starvation conditions. *Curr. Microbiol*. 58: 541-546.
829
830 Naik MT, Suree N, Ilangovan U, Liew CK, Thieu W, Campbell DO, Clemens JJ, Jung ME,
831 Clubb RT (2006) Staphylococcus aureus Sortase A transpeptidase – Calcium promotes sorting
832 signal binding by altering the mobility and structure of an active site loop. *Journal of Biological*
833 *Chemistry* 281: 1817-1826.
834
835 Nies DH (2007) Bacterial transition metal homeostasis. In Molecular Microbiology of Heavy
836 Metals, DH Nies and S Silver (eds), Microbiology Monographs 6, pp 117-142.
837
838 Nilsson HJ, Tyliszczak T, Wilson RE, Werme L, Shuh DK (2005) Soft X-ray scanning
839 transmission X-ray microscopy (STXM) of actinide particles. *J. Anal. Bioanal. Chem*. 383: 41-
840 47 (2005). DOI: 10.1007/s00216-005-3355-5
841
842 Ortiz-Bernad I, Anderson RT, Vrionis HA and Lovley DR (2004a) Vanadium respiration by
843 Geobacter metallireducens: Novel strategy for in situ removal of vanadium from groundwater.
844 *Appl. Environ. Microbiol.* 70: 3091-3095.

Ortiz-Bernad I, Anderson RT, Vrionis HA and Lovley DR (2004b) Resistance of solid-phase U(VI) to microbial reduction during *in situ* bioremediation of uranium-contaminated groundwater. *Appl. Environ. Microbiol*. 70: 7558-7560.

Premovic PI, Pavlovic MS and Pavlovic NZ (1986) Vanadium in ancient sedimentary rock of marine origin. *Geochim. Cosmochim. Acta* 50: 1923-1931.

Rehder D. Bioinorganic Vanadium Chemistry. John Wiley & Sons, Chichester, 2008.

Smeaton CM, Weisener CG, Burns PC, Fryer BJ, Fowle DA (2008) Bacterially enhanced dissolution of meta-autunite. *American Mineralogist* 93: 1858-1864.

Spirakis, CS (1996) The roles of organic matter in the formation of uranium deposits in sedimentary rocks. *Ore Geology Reviews* 11: 53-69.

Stern TW, Stieff LR, Girhard MN, Meyrowitz R (1956) The occurrence and properties of meta-tyuyamunite, $Ca(UO_2)_2(VO_4)_2 \cdot 3\text{-}5H_2O$. *American Mineralogist* 41:187-201.

Stohl FV and Smith DK (1981) The crystal chemistry of the uranyl silicate minerals. *Am. Mineral* 66:610-625.

Stylo M, Alessi DS, Shao PP, Lezama-Pacheco JS, Bargar JR, Bernier-Latmani R (2013) Biogeochemical controls on the product of microbial U(VI) reduction. *Environ. Sci. Technol*. 47: 12351-12358.

Thews, KB and Heinle FJ (1923) Extraction and recovery of radium, vanadium and uranium from carnotite. Industrial and Engineering Chemistry 15: 1159-1161.

Tokunaga TK, Kim Y and Wan JM (2009) Potential remediation approach for uranium-contaminated groundwaters through potassium uranyl vanadate precipitation. *Environ. Sci. Technol.* 43: 5467-5471.

Tokunaga TK, Kim Y, Wan JM, Yang L (2012) Aqueous uranium (VI) concentrations controlled by calcium uranyl vanadate precipitates. *Environ. Sci. Technol*. 46: 7471-7477.

Urrutia MM, Roden EE, Fredrickson JK, Zachara JM. (1998) Microbial and surface chemistry controls on reduction of synthetic Fe(III) oxide minerals by the dissimilatory iron-reducing bacterium Shewanella alga. *Geomicrobiol. J.* 15: 269-291.

Van der Laan G, Moore K T, Tobin J G, Chung B W, Wall M A, Schwartz A J (2004) *Phys Rev Lett* 93:097401

Vrionis HA, Anderson RT, Ortiz-Bernad I, O'Neill KR, Resch CT, Peacock AD, Dayvault R, White DC, Long PE, Lovely DR (2005) Microbiological and geochemical heterogeneity in an *in situ* uranium bioremediation field site. *Appl. Environ. Microbiol*. 71: 6308-6318.

892 Weeks, AD (1961) Mineralogy and geochemistry of vanadium in the Colorado Plateau. *Journal*
893 *of the Less-Common Metals* 3: 443-450.
894
895 Wehrli B and Stumm W (1989) Vanadyl in natural waters: Adsorption and hydrolysis promote
896 oxygenation. *Geochim. Cosmochim. Acta* 53: 69-77.
897
898 Wen X-D, Löble MW, Batista ER, Bauer E, Boland KS, Burrell AK, Conradson SD, Daly SR,
899 Kozimor SA, Minasian SG, Martin RL, McCleskey TM, Scott BL, Shuh DK, Tyliszczak T,
900 Electronic Structure and O K-edge XAS Spectroscopy of U_3O_8,. *J. Electron Spectros. Rel.*
901 *Phenom.* 194: 81-87 (2014). DOI: 10.1016/j.elecspec.2014.03.005
902
903 Wiegand I., Hilpert K., Hancock, R. E. W. (2008) Agar and broth dilution methods to determine
904 the minimum inhibitory concentration (MIC) of antimicrobial substances. *Nature Protocols* 3 (2):
905 163-175.
906
907 Williams K.H., Long P.E., Davis J.A., Wilkins M.J., N'Guessan A.L., Steefel C.I., Yang L.,
908 Newcomer D., Spane F.A., Kerkhof L.J., McGuinness L., Dayvault R. and Lovley D.R. (2011)
909 Acetate Availability and its Influence on Sustainable Bioremediation of Uranium-Contaminated
910 Groundwater, *Geomicrobiology Journa*l 28: 5-6, 519-539.
911
912 Wu ZY, Jollet F, Gota S, Thromat N, Gautier-Soyer M, Petit T (1999) X-ray absorption at the
913 oxygen K edge in cubic f oxides examined using a full multiple-scattering approach. *J. Phys.*
914 *Condens. Matter* 11: 7185-7194.
915
916 Xu J, Veeramani H, Qafoku NP, Singh G, Riquelme MV, Pruden A, Kukkadapu RK, Gartman
917 BN, Hochella MF (2017) Efficacy of acetate-amended biostimulation for uranium sequestration:
918 Combined analysis of sediment/groundwater geochemistry and bacterial community structure.
919 *Appl. Geochem.* 78: 172-185.
920
921 Yang Y, Wang S, Albrecht-Schmitt TE (2014) Microbial dissolution and reduction of uranyl
922 crystals by *Shewanella oneidensis* MR-1. *Chemical Geology* 387: 59-65.
923
924 Yang U, Saiers JE, Xu N, Minasian SG, Tyliszczak T, Kozimor SA, Shuh DK, Barnett MO.
925 2012. Impact of natural organic matter on uranium transport through saturated geologic materials:
926 from molecular to column scale. *Enviro. Sci. Technol.* 46: 5931-5938.
927
928 Yelton A.P., Williams K.H., Fournelle J., Wrighton K.C., Handley K.M., Banfield J.F. Vanadate
929 and Acetate Biostimulation of Contaminated Sediments Decreases Diversity, Selects for Specific
930 Taxa, and Decreases Aqueous V5+ Concentration. *Enviro. Sci. Technol.* 47: 6500–6509.
931
932 Zachara JM, Fredrickson JK, Li SM, Kennedy DW, Smith SC, Gassman PL (1998) Bacterial
933 reduction of crystalline Fe3+ oxides in single phase suspensions and subsurface materials. *Am.*
934 *Mineral.* 83:1426-1443.
935
936 Zhuang K., Ma E., Lovley DR, Mahadevan R. (2012) The design of long-term effective uranium
937 bioremediation strategy using a community metabolic model. *Biotechnology and Bioengineering*
938 109: 2475-2483.

939 Table 1. Element concentrations for separated fine yellow particles of uranium ore and
940 fine mineral fraction after incubation with *S. putrefaciens.* The standard deviation for.
941 triplicate samples was less than 5%.
942
943
944

Element	U-ore, mg/kg	Incubated U-ore, mg/kg
U	301384	293880
V	73458	66615
Na	134	1805
K	832	4402
Ca	19940	5440
Mg	1296	1669
Ba	1778	1498
Fe	3930	5145
Mn	3643	3303

945
946

FIGURE CAPTIONS

Figure 1. a) Grain of quartz sand coated with U- and V-containing minerals observed by scanning electron microscopy and energy dispersive spectroscopy b) X-ray diffractograms of the separated sand (upper), fine yellow U-containing solids (tyuyamunite; middle) and fine clay material separated after incubation with *S. putrefaciens* CN32. Continuous lines represent results of whole pattern fitting.

Figure 2. Changes in solution concentrations of V and U. Concentrations of dissolved vanadium (a) and uranium (b) during anaerobic respiration of *S. putrefaciens* CN32 in the presence of carnotite.Concentrations of dissolved vanadium (c) and uranium (d) during incubation with a mixed solution containing soluble V(V) and U(VI) at 1 mM concentrations. Open diamonds represent treatments inoculated with CN32; filled diamonds are bacteria-free control treatments.

Figure 3. Transmission electron micrographs showing the association of CN32 with U-ore minerals. a) and b) thin sections of cultures after 3 days; c) whole mount preparation of culture after 3 days; d) whole mount preparation of 4-month culture. Arrows indicate bacteria; scale bars are 500 μm (a, c, d) and 250 μm (b).

Figure 4. STXM-derived Vanadium 2p core absorption spectra (left) and Uranium 4d core spectra (right) showing changes during incubation with *S. putrefaciens* CN32. V $L_{2,3}$ absorption maxima shift to lower energy values with reduction from V^{5+} to V^{4+} in the range from 514-520 eV (dashed line, left) and 524-526 eV. U d absorption maxima shift around 1.3 eV to lower energy with reduction from U(VI) to U(IV), from 780 eV to 778.7 eV (N_4 edge), and from 738 eV to around 737 (N_5 edge) (dashed lines, right), which was not observed for the U-ore treatments.

Figure 5. Changes over time in the spatial distribution of uranium and vanadium during incubation of *S. putrefaciens* with uranium ore, as shown by scanning transmission X-ray microscopy. After 3 days: a) STXM image recorded at 518.5eV showing bacteria and particles b) chemical map indicating colocalization of V(V) and U(VI) and. After 4 months: c) STXM image recorded at 518.5eV and d) corresponding chemical map showing distinct V(V) and U(VI) phases and e) chemical map evidencing V(V) and V(IV), derived from stack fitting using larger pixel size. U(VI) is mainly colocalized with V(IV) and not with V(V). f) STXM image recorded at 518.5eV at 4 months and g) corresponding V map (derived from a "stack") showing that bacteria contain vanadium. Uranium was not detected on the cells. See corresponding spectra in Fig. 4. Arrows point to bacteria. Scale bars are 1 μm.

Figure 6. STXM-derived elemental distribution and chemical speciation of vanadium and uranium in CN32 samples during the reduction of soluble V, U after three days. a) STXM image recorded at 307 eV. Elemental maps showing b) carbon in red, vanadium in green, c) carbon in red, uranium in green. d and e) U $N_{4,5}$ edges NEXAFS spectra showing that U is present as U(IV).

Figure 7. Biofilm formation of *S. putrefaciens* CN32 and *E. coli* K-12 in response to U(VI) (a,d); V(IV) (b, e) and Ca (c, f). The amount of retained crystal violet stain indicates the amount of biomass adhered to the sides of the glass tubes after 20 h incubation in the presence/absence of added elements.

Appendix A: STXM image recorded at 738 eV (U N5 -edge) and STXM-derived elemental maps of 8 carnotite after incubation with CN32 for 8 months. Scale bars are 2 microns.

Appendix B. STXM-derived elemental maps (at C K and U $N_{4,5}$ edges) of hydrated samples after 1 week incubation with U ore, showing abundant C matrix with potassium associated with embedded bacterial cells (a). The bacteria are not strongly associated with U (b). Scale bars are 500 μm. Arrows point to cells.

Appendix C. Minerals containing U and P formed during the incubation of CN32 with uranium sandstone ore.

Appendix D. STXM-derived VL2,3 and O-K edges NEXAFS spectra of CN32 samples during the reduction of soluble V, U after three days suggesting the presence of V(III).

a

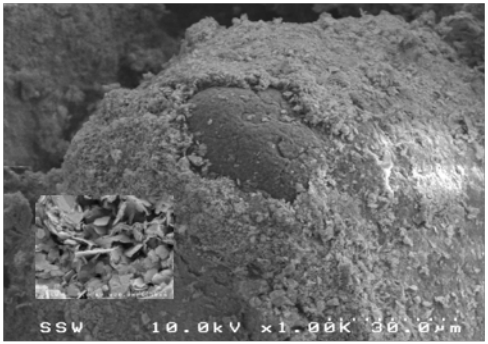
SSW 10.0kV x1.00k 30.0µm

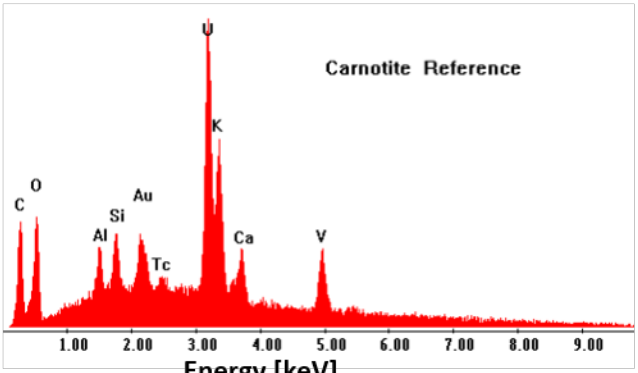
Carnotite Reference
U
K
C
O
Au
Si
Al
Tc
Ca
V
1.00
2.00
3.00
4.00
5.00
6.00
7.00
8.00
9.00
Energy [keV]

b

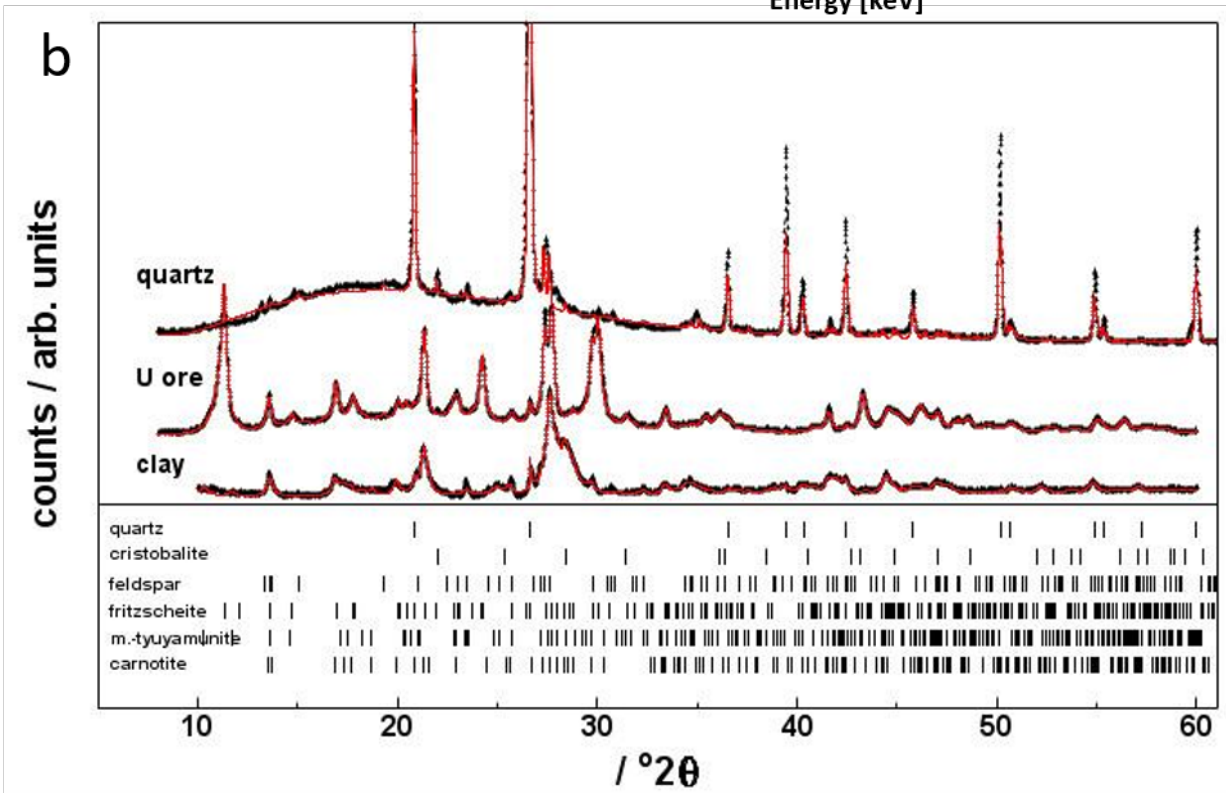
counts / arb. units
quartz
U ore
clay
quartz
cristobalite
feldspar
fritzscheite
m.-tyuyamunite
carnotite
10
20
30
40
50
60
/ °2θ

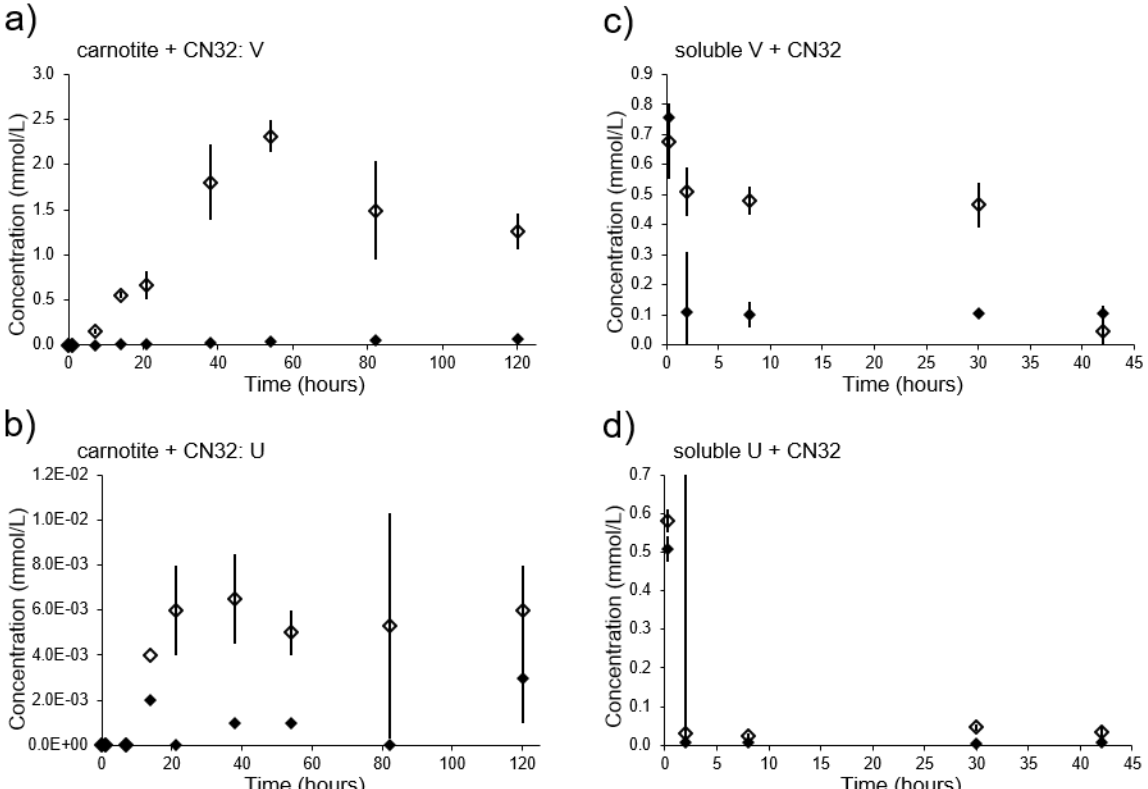
a)
carnotite + CN32: V
Concentration (mmol/L)
Time (hours)
b)
carnotite + CN32: U
Concentration (mmol/L)
Time (hours)
c)
soluble V + CN32
Concentration (mmol/L)
Time (hours)
d)
soluble U + CN32
Concentration (mmol/L)
Time (hours)

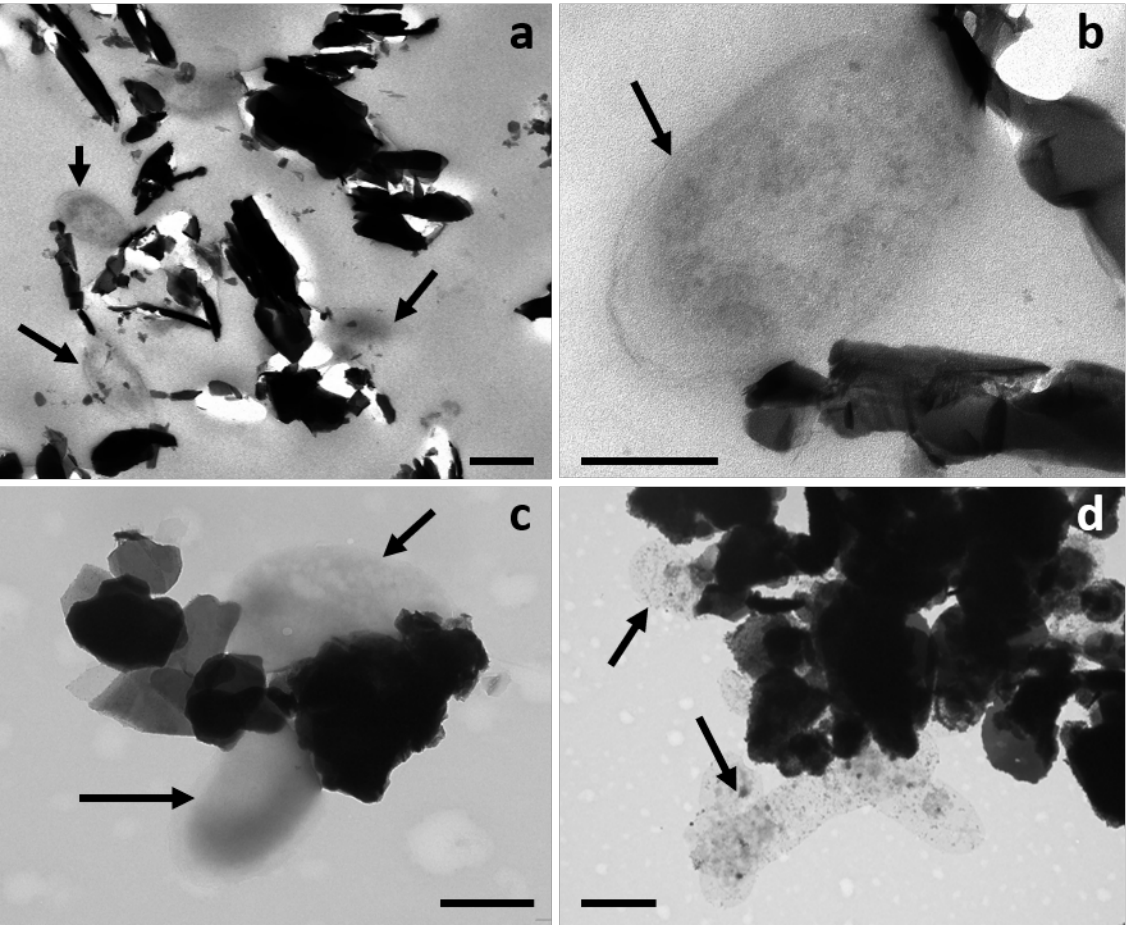
a
b
c
d

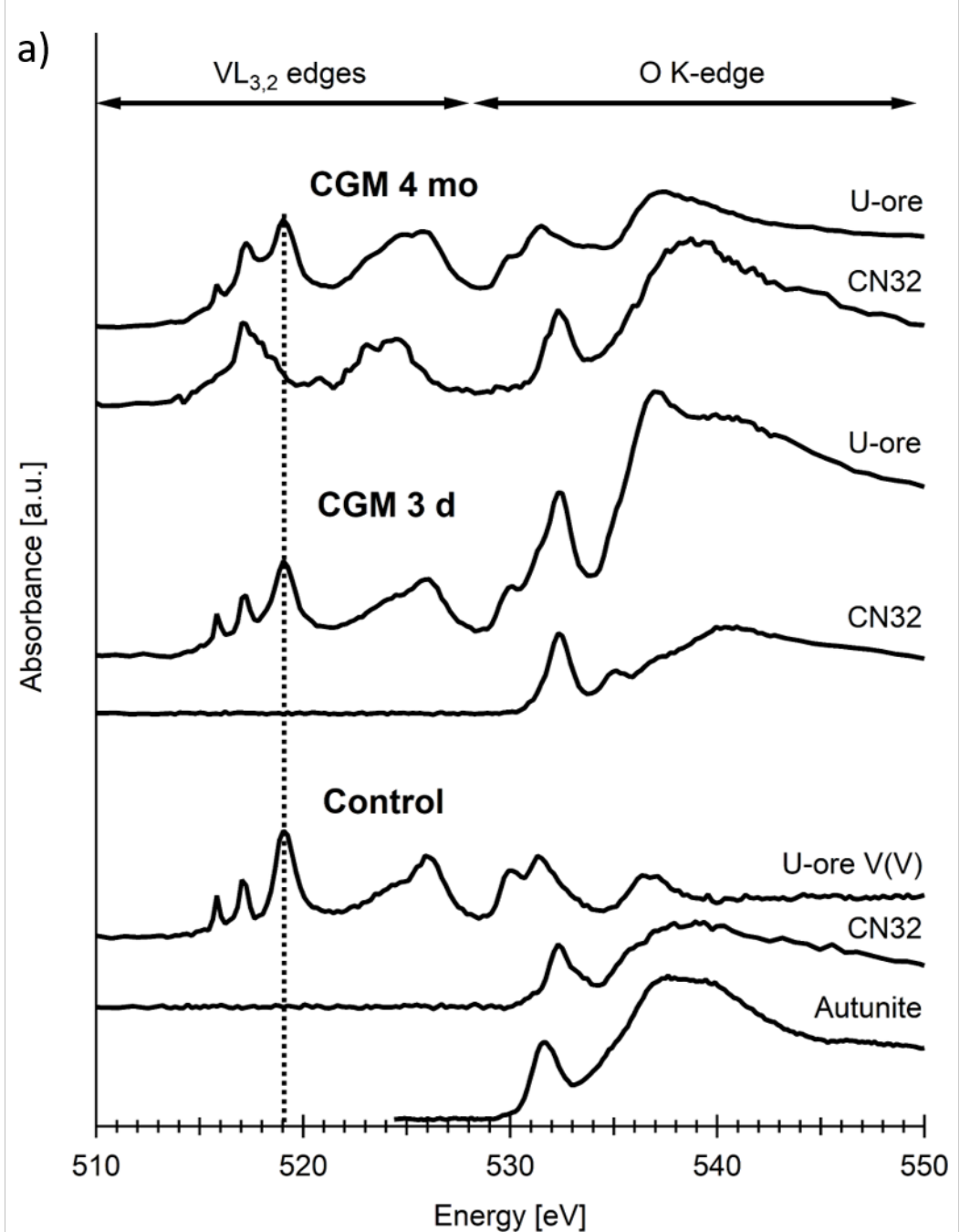
a)
VL3,2 edges
O K-edge
CGM 4 mo
U-ore
CN32
CGM 3 d
U-ore
CN32
Control
U-ore V(V)
CN32
Autunite
Absorbance [a.u.]
510
520
530
540
550
Energy [eV]

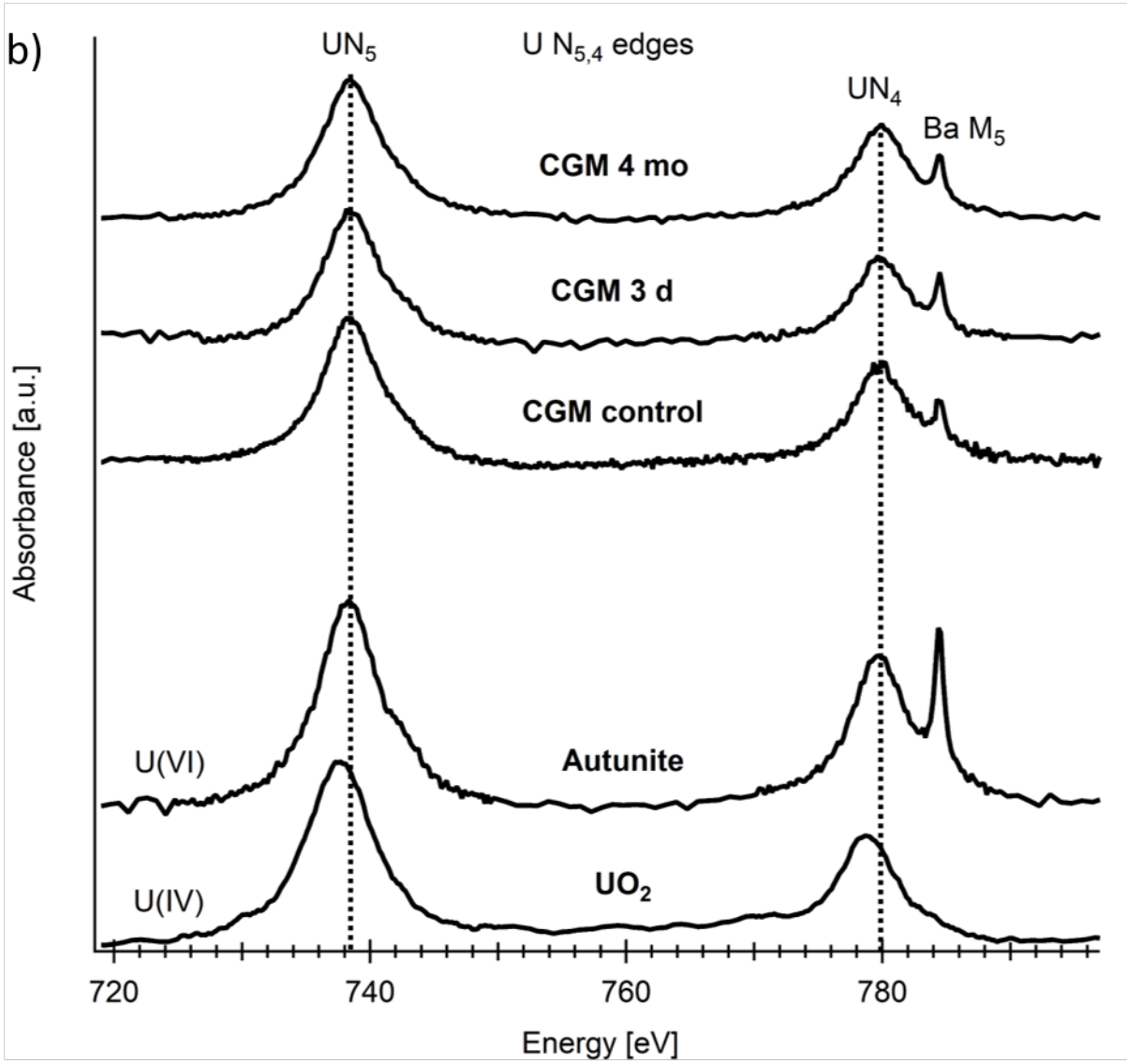
b)
UN5
U N5,4 edges
UN4
Ba M5
CGM 4 mo
CGM 3 d
CGM control
U(VI)
Autunite
U(IV)
UO2
Absorbance [a.u.]
720
740
760
780
Energy [eV]

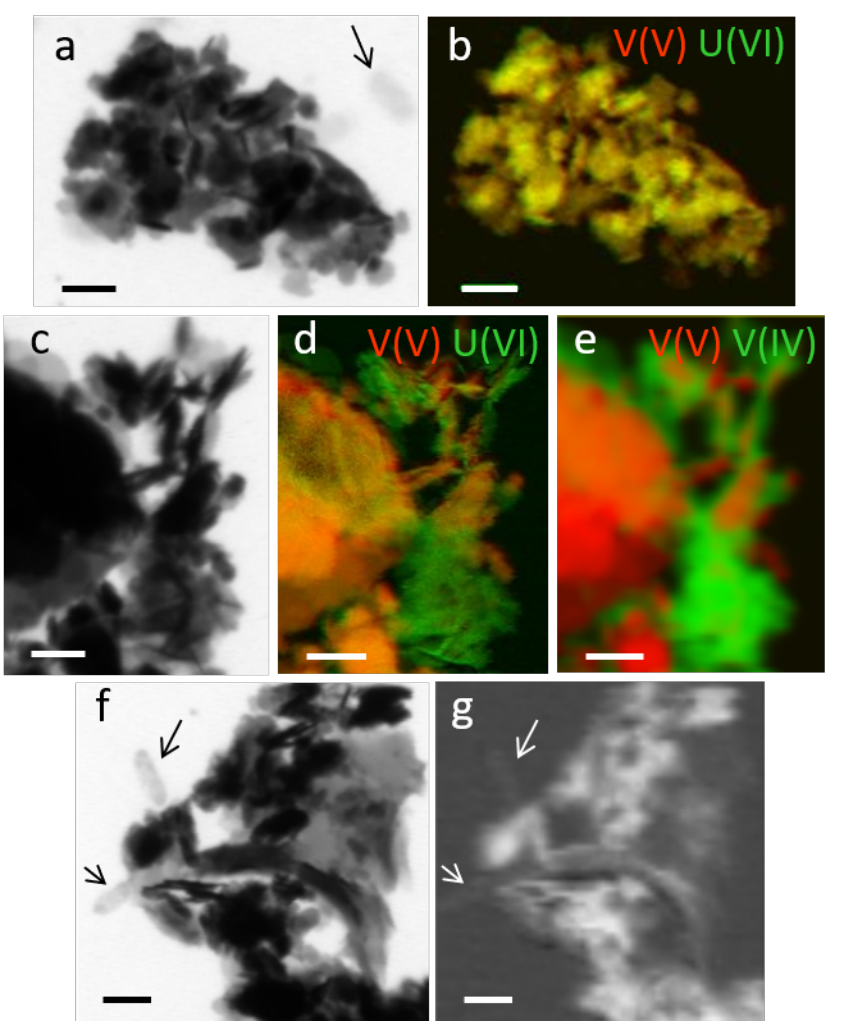
a
b
V(V) U(VI)
c
d
V(V) U(VI)
e
V(V) V(IV)
f
g

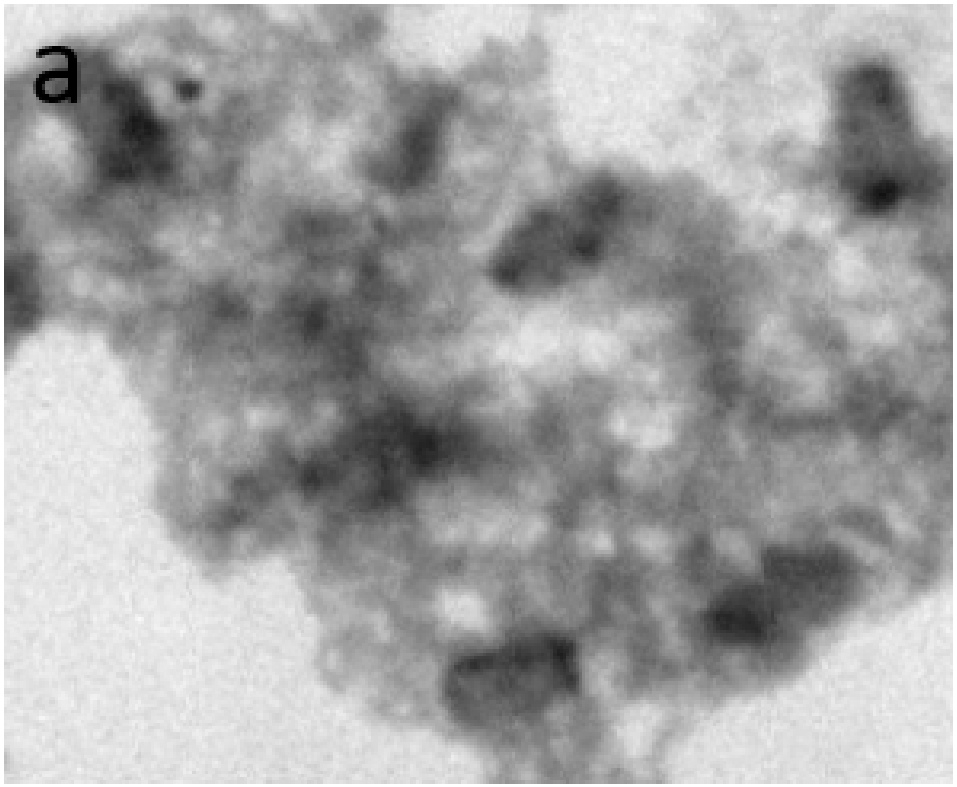
a

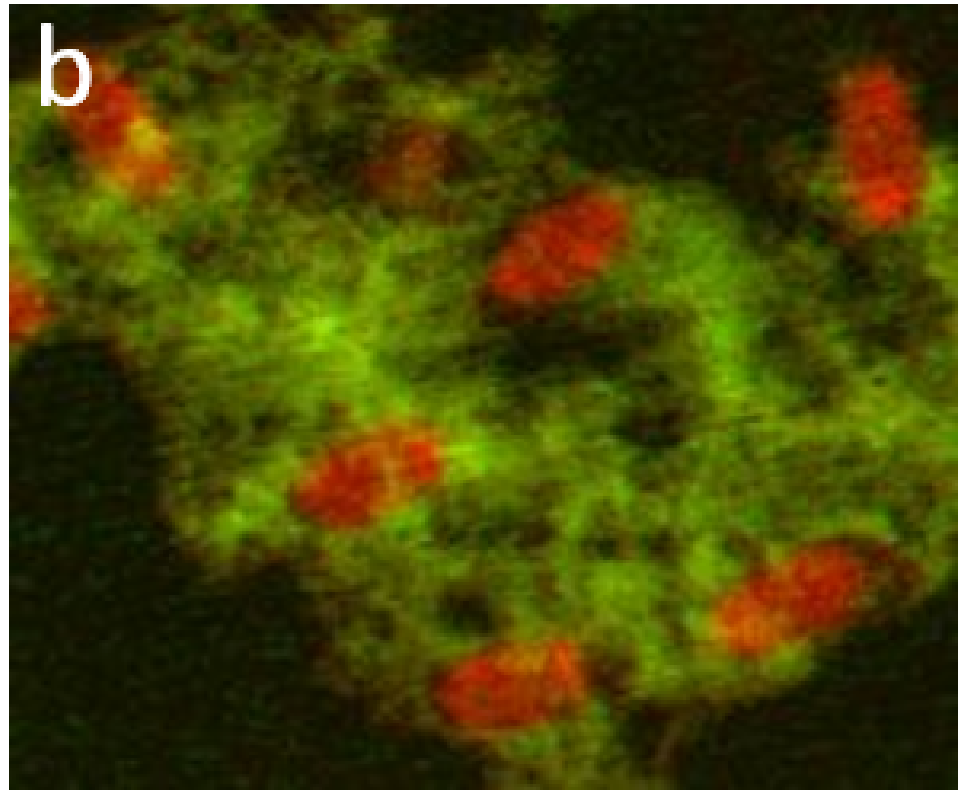
b

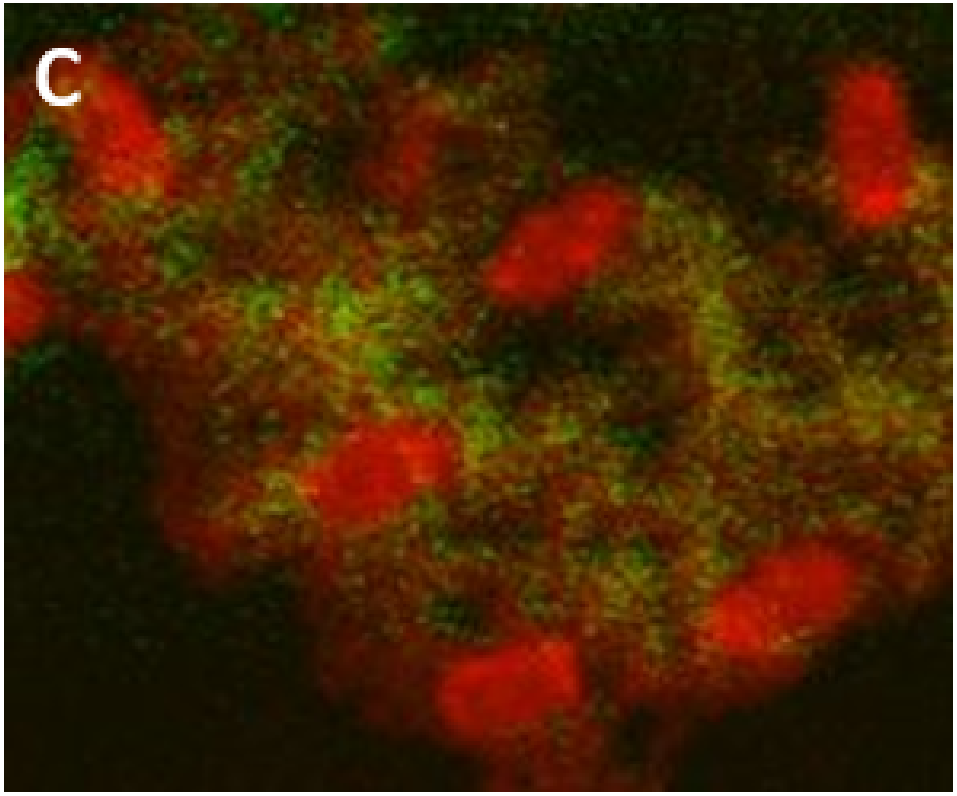
c

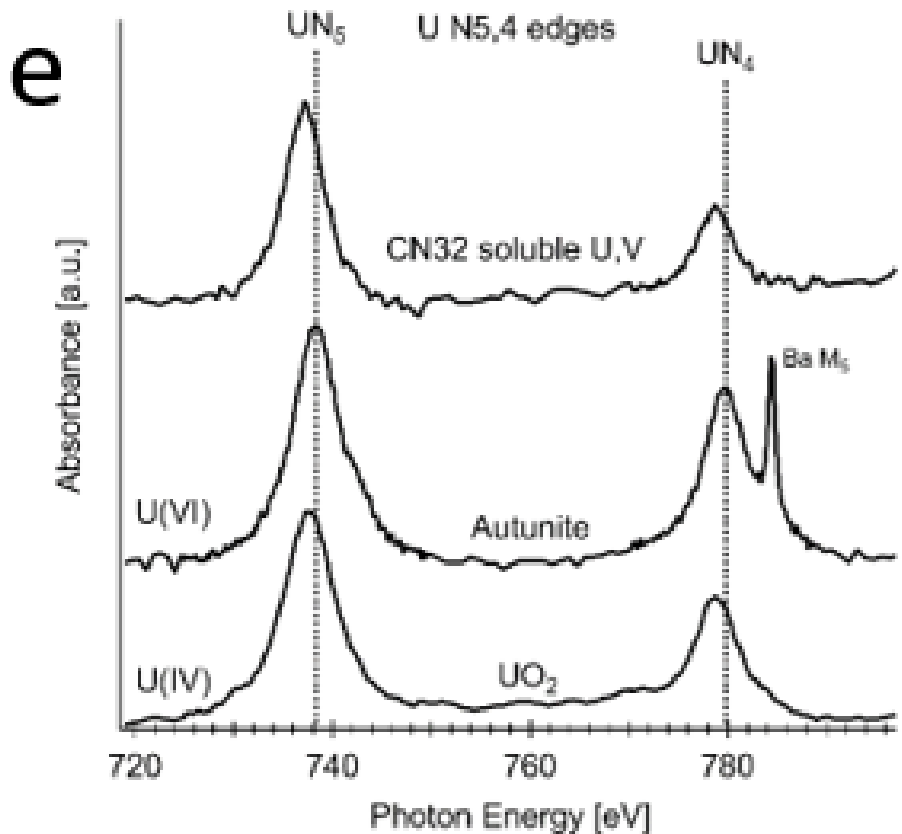
e
U N5,4 edges
UN5
UN4
CN32 soluble U,V
Ba M5
U(VI)
Autunite
U(IV)
UO2
Absorbance [a.u.]
720
740
760
780
Photon Energy [eV]

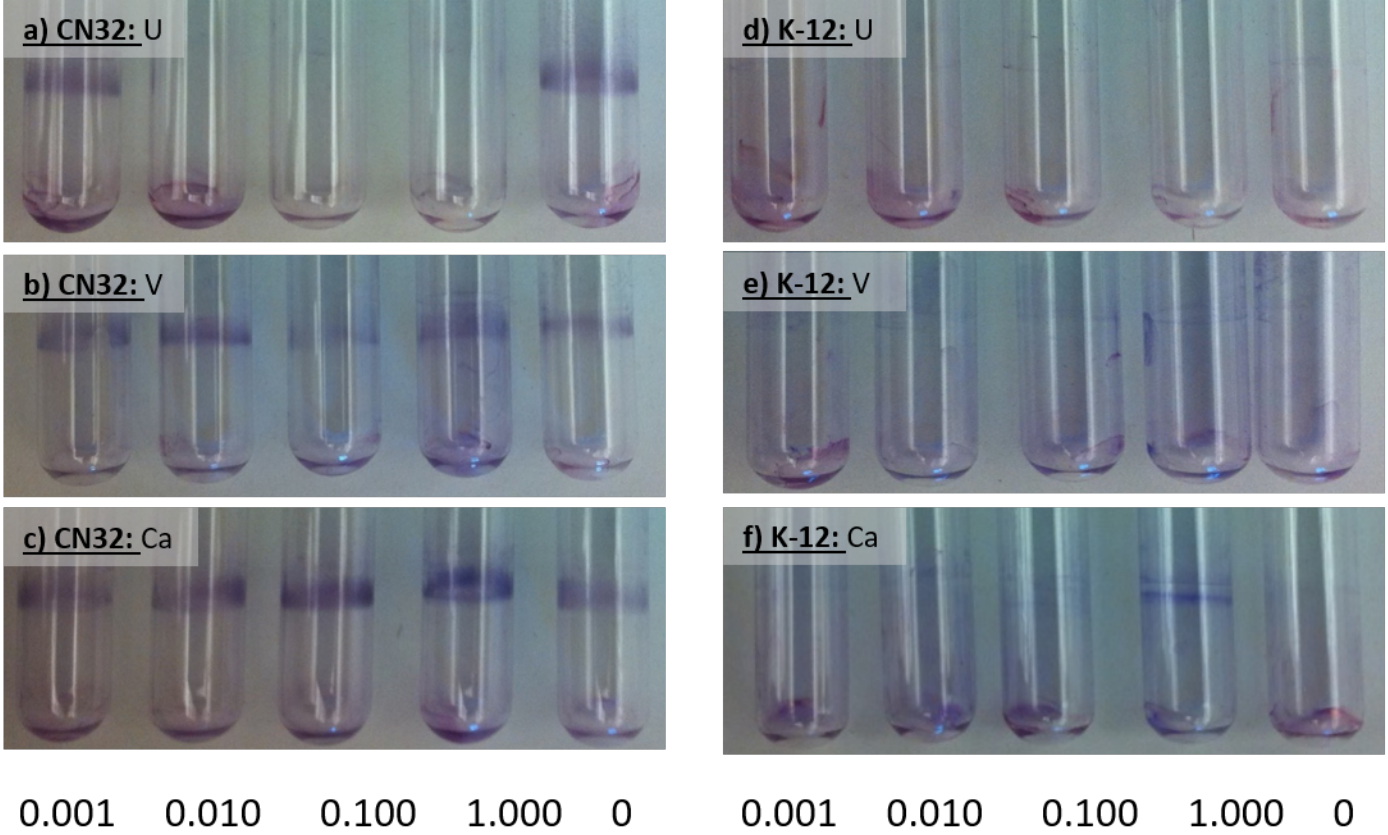
a) CN32: U
d) K-12: U
b) CN32: V
e) K-12: V
c) CN32: Ca
f) K-12: Ca
0.001 0.010 0.100 1.000 0
0.001 0.010 0.100 1.000 0
Concentration of element (mM)